Rabies virus P protein binds to TBK1 and interferes with the formation of innate immunity-related liquid condensates

Nathalie Scrima, Romain Le Bars, Quentin Nevers, Damien Glon, Guillaume Chevreux, Ahmet Civas, Danielle Blondel, Cécile Lagaudrière-Gesbert, Yves Gaudin

Cell Reports

Article

Rabies virus P protein binds to TBK1 and interferes with the formation of innate immunity-related liquid condensates

Graphical abstract

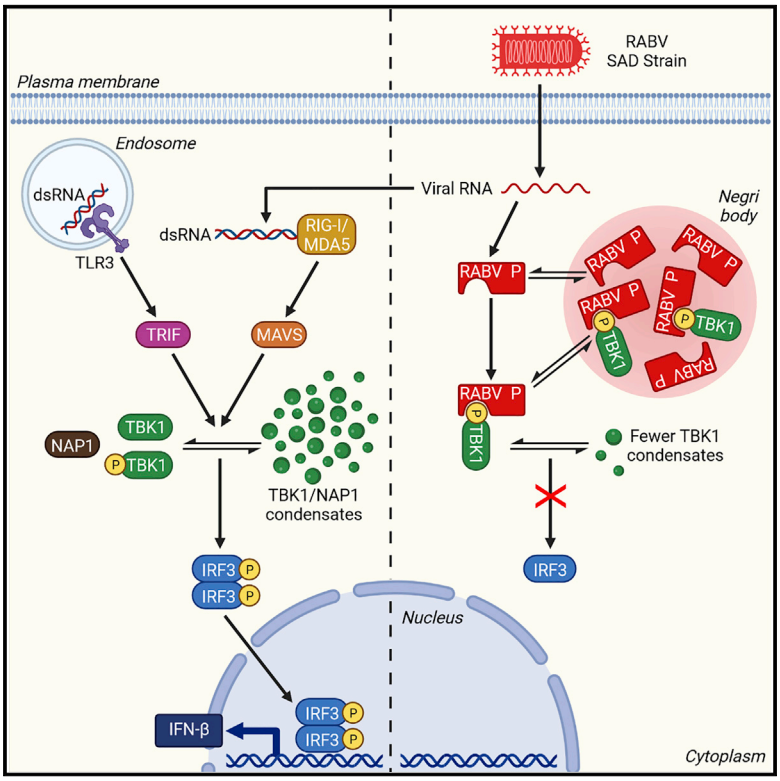

Highlights

- Upon interferon-inducing signals, TBK1, NAP1, and SINTBAD form liquid condensates
- Rabies virus phosphoprotein P binds TBK1 to inhibit interferon induction pathways
- A change of serine 179 to proline abolishes the P-inhibitory activity
- Mutations of TBK1 phosphorylation sites abolish P binding

Authors

Nathalie Scrima, Romain Le Bars, Quentin Nevers, ..., Danielle Blondel, Cécile Lagaudrière-Gesbert, Yves Gaudin

Correspondence

cecile.lagaudriere@i2bc.paris-saclay.fr (C.L.-G.), yves.gaudin@i2bc.paris-saclay.fr (Y.G.)

In brief

Scrima et al. show that rabies virus (RABV) phosphoprotein P binds to phosphorylated TBK1, the kinase phosphorylating IRF3, and thus inhibits interferon induction. Upon RABV infection or dsRNA detection by innate immunity sensors, TBK1, NAP1, and SINTBAD form liquid condensates. The P-TBK1 association interferes with the formation of these condensates.

Scrima et al., 2023, Cell Reports *42*, 111949
January 31, 2023
https://doi.org/10.1016/j.celrep.2022.111949

CellPress

Cell Reports

CellPress
OPEN ACCESS

Article

Rabies virus P protein binds to TBK1 and interferes with the formation of innate immunity-related liquid condensates

Nathalie Scrima,[1] Romain Le Bars,[1,3] Quentin Nevers,[1,3] Damien Glon,[1,3] Guillaume Chevreux,[2] Ahmet Civas,[1] Danielle Blondel,[1] Cécile Lagaudrière-Gesbert,[1,4,*] and Yves Gaudin[1,4,5,*]
[1]Institute for Integrative Biology of the Cell (I2BC), CEA, CNRS, Université Paris-Saclay, 91198 Gif-sur-Yvette, France
[2]Institut Jacques Monod, Université de Paris, CNRS, 75013 Paris, France
[3]These authors contributed equally
[4]These authors contributed equally
[5]Lead contact
*Correspondence: cecile.lagaudriere@i2bc.paris-saclay.fr (C.L.-G.), yves.gaudin@i2bc.paris-saclay.fr (Y.G.)
https://doi.org/10.1016/j.celrep.2022.111949

SUMMARY

Viruses must overcome the interferon-mediated antiviral response to replicate and propagate into their host. Rabies virus (RABV) phosphoprotein P is known to inhibit interferon induction. Here, using a global mass spectrometry approach, we show that RABV P binds to TBK1, a kinase located at the crossroads of many interferon induction pathways, resulting in innate immunity inhibition. Mutations of TBK1 phosphorylation sites abolish P binding. Importantly, we demonstrate that upon RABV infection or detection of dsRNA by innate immunity sensors, TBK1 and its adaptor proteins NAP1 and SINTBAD form dynamic cytoplasmic condensates that have liquid properties. These condensates can form larger aggregates having ring-like structures in which NAP1 and TBK1 exhibit locally restricted movement. P binding to TBK1 interferes with the formation of these structures. This work demonstrates that proteins of the signaling pathway leading to interferon induction transiently form liquid organelles that can be targeted by viruses.

INTRODUCTION

The host interferon (IFN) response constitutes a barrier that viruses must overcome to establish a productive infection.[1,2] The IFNs are expressed and secreted following microbe-associated molecular patterns (MAMPs) recognition by dedicated cellular proteins known as pattern recognition receptors (PRRs). Subsequent binding of IFNs to their receptors, leads to the upregulation of hundreds of IFN-stimulated genes (ISGs) that establish an antiviral state to limit further viral replication and spread.[3] Two subsets of PRRs, the Toll-like receptors (TLRs) and the RIG-I-like receptors (RLRs), are involved in recognition of RNA viruses.[4]

TLRs are transmembrane proteins that reside either at the cell surface or in endosomal compartments.[5] TLR3, which recognizes double-stranded RNA (dsRNA), is a key player in the detection of RNA viruses.[6,7] RNA binding by TLR3 activates a signaling cascade that leads to TANK-binding kinase 1 (TBK1)-mediated phosphorylation of transcription factors IRF3 and/or IRF7[8,9] resulting in their homo- or heterodimerization, which induces type I IFN-related genes.[1]

RIG-I and MDA-5 are cytosolic receptors recognizing non-self RNAs in the cell cytoplasm.[10] RIG-I is activated by short stretches of 5′ppp or 5′pp dsRNA,[11] while MDA-5 is activated by longer stretches of dsRNA in a 5′ phosphate-independent manner.[12] They are helicases that both contain two caspase activation and recruitment domains (CARDs) at their N terminus. RNA binding triggers a structural transition in the RLRs resulting in CARDs exposure[11,12] and association with the mitochondrial antiviral signaling protein (MAVS) at the outer mitochondrial membrane.[13] This interaction induces MAVS oligomerization and assembly of complexes that activate TBK1 kinase activity,[14,15] resulting in IRF3 and/or IRF7 phosphorylation, their homo- or heterodimerization, and consequently the expression of type I IFNs.

RNA viruses have evolved strategies that counteract IFN induction, IFN signaling, and ISGs activity.[16] Rabies virus (RABV) is a neurotropic virus that causes fatal disease in humans and animals.[17] RABV is a member of the Rhabdoviridae family (Mononegavirales [MNV] order) and its genome consists of a negative sense, single-stranded RNA. RABV genome transcription and replication take place within Negri bodies (NBs) that are cytoplasmic spherical structures formed during viral infection, having 1 to 5 μm diameter and enriched in the viral nucleoprotein N, the RNA-dependent RNA polymerase L and its cofactor, the phosphoprotein P.[18] NBs have been demonstrated to have liquid properties and are formed by liquid-liquid phase separation (LLPS)[19] like several other MNV viral factories.[20–24]

RABV P is the major viral counteractant of the innate immune response.[25,26] First, P has a critical role in suppression of IFN

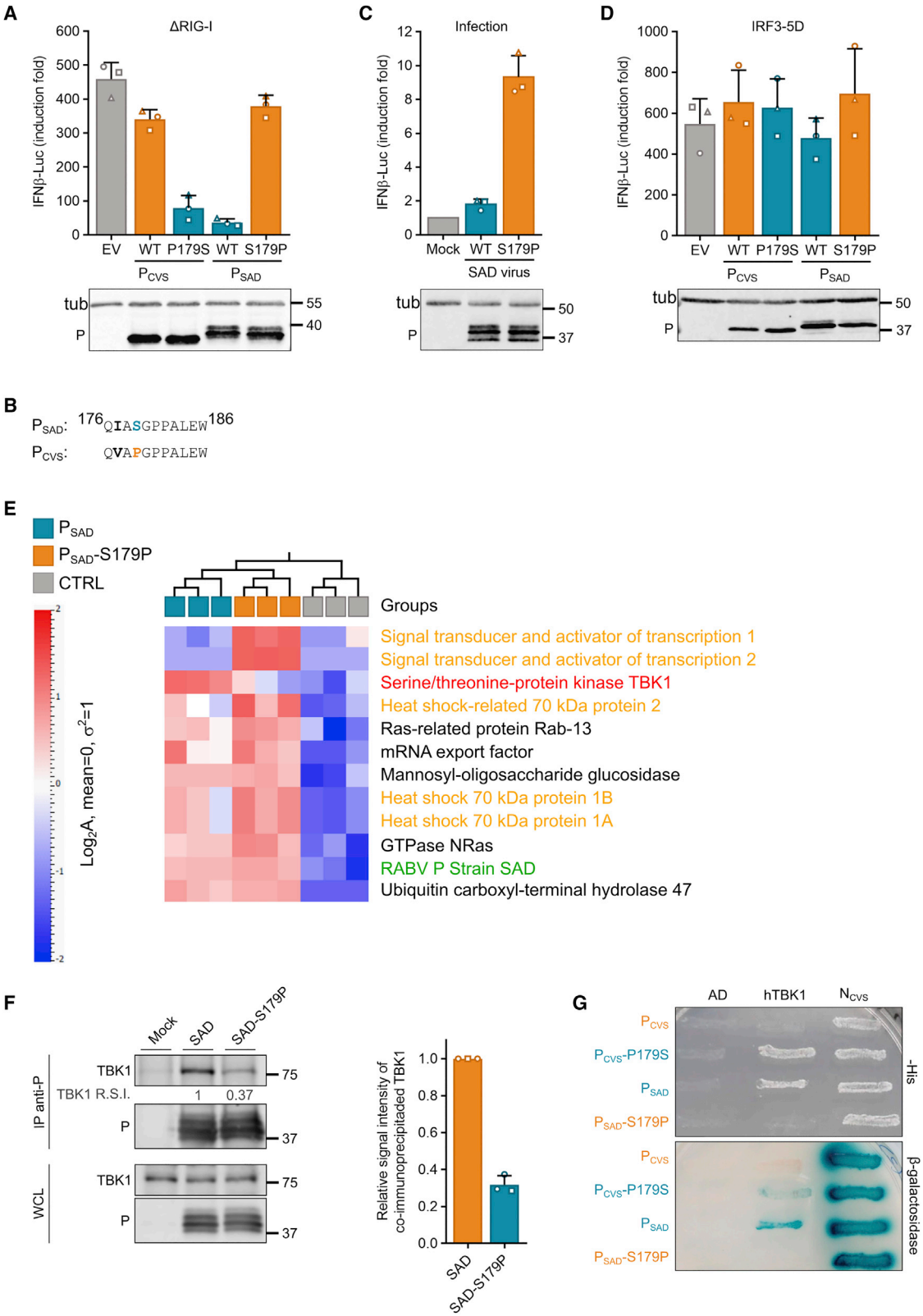

(legend on next page)

CellPress
OPEN ACCESS

production by blocking the phosphorylation of IRF3 by TBK1 through a mechanism that is not elucidated.[27] Second, the interaction of P with STAT1 leads to the inhibition of IFN signaling.[28–30] Finally, P interacts with the promyelocytic leukemia protein (PML),[31] an ISG, and consequently counteracts the antiviral effect of isoform PML IV against RABV.[32]

In this study, we investigated how RABV P blocks IRF3 phosphorylation. We took advantage of the distinct phenotype of two RABV strains (SAD and CVS) relative to their ability to inhibit IFN induction. We demonstrated that P_{SAD}, but not P_{CVS}, inhibits IFN induction. A single amino acid residue substitution in position 179 is responsible for the phenotype difference observed between the two strains. Therefore, a recombinant SAD-S179P (in which P_{SAD} is replaced by its S179P version) shows a growth defect in IFN-producing cells. Using protein mass spectrometry, we identified TBK1 as a protein that preferentially interacts with the inhibitory forms of P. Consequently, TBK1 is partly concentrated in NBs in N2A cells. Mutations of TBK1 phosphorylation sites S172 and Y179 abolish P binding and TBK1 concentration in NBs. More importantly, upon RABV infection, TBK1 together with its adaptor proteins NAP1 and SINTBAD forms cytoplasmic, dynamic condensates. We show that TBK1 and NAP1 condensates have liquid properties. TBK1 condensates are also formed upon detection of dsRNA by innate immunity sensors and P binding to TBK1 interferes with the formation of these condensates. This work demonstrates that proteins of the signaling pathway leading to IFN production transiently form liquid organelles that can be targeted by viruses.

RESULTS

P_{SAD} but not P_{CVS} inhibits IFN induction

RABV P protein (SAD strain) is responsible for inhibition of IFN induction in infected cells.[27] Using a reporter gene assay, in which a plasmid-encoded luciferase gene is controlled by the IFN-β promoter, we compared the inhibitory effect of P_{SAD} and P_{CVS} in human embryonic kidney 293T (HEK293T) cells. Promoter activity was induced by expression of a constitutively active form of RIG-I (ΔRIG-I corresponding to protein residues 1–228)[33] (Figure 1A). Consistent with previous results, P_{SAD} efficiently inhibited IFN induction.[27] This inhibition was not observed with P_{CVS} (Figure 1A).

As the P domain from amino acid residues 176–186 had been suggested to be involved in the inhibition,[34] we compared P_{CVS} and P_{SAD} sequences in this region. Sequence alignment reveals two amino acid changes in positions 177 (Ile in SAD versus Val in CVS) and 179 (Ser in SAD versus Pro in CVS) (Figure 1B).

The single replacement of proline 179 by a serine in CVS restored P ability to inhibit IFN induction (Figure 1A). Conversely, replacement of serine 179 by a proline in P_{SAD} abolished its inhibitory properties (Figure 1A).

We then constructed a recombinant SAD virus in which P_{SAD} is replaced by its S179P version (SAD-S179P). We compared one-step (MOI = 3) and multiple-step (MOI = 0.05) growth curves in BSR, N2A, and U-373MG cell lines. Although there was no significant difference in the multiplication of SAD and SAD-S179P in BSR and N2A cell lines, the production of SAD-S179P decreased by more than one $\log_{10}$ after 72 h of infection at low MOI in U-373MG (Figure S1A).

We then analyzed the impact of infection with SAD and SAD-S179P on the IFN pathway induction, either indirectly using the luciferase assay in HEK293T cells, or directly by quantifying IFN-β mRNAs in N2A and U-373MG cells (Figures 1C and S1B). In both HEK293T and U-373MG, there was a significant induction of IFN-β upon infection by SAD-S179P but not by SAD (Figures 1C and S1B). This induction began between 8 and 12 h post-infection (p.i.) in U-373MG (Figure S1B). Accordingly, in SAD-infected U-373MG cells, IRF3 remains in the cytoplasm,

Figure 1. P protein of RABV SAD strain (but not that of CVS strain) inhibits IFN production by binding TBK1

(A) IFN induction inhibition by P_{CVS}, P_{SAD}, P_{CSV}-P179S, and P_{SAD}-S179P assessed using the luciferase assay. HEK293T cell lysates were analyzed using western blot (WB) with anti-P and anti-tubulin antibodies. The bars represent the mean fold induction of firefly luciferase compared with unstimulated cells (not transfected with pEF6FLAGΔRIG-I). EV, empty vector. Data points represent 3 independent experiments. Error bars indicate SD.

(B) Amino acid differences between P_{CVS} and P_{SAD} in region 176–186.

(C) IFN induction inhibition by SAD and SAD-S179P assessed using the luciferase assay. HEK293T cell lysates were analyzed using WB with anti-P and anti-tubulin antibodies. The bars represent the mean fold induction of firefly luciferase compared with that in mock-infected cells. Data points represent 3 independent experiments. Error bars indicate SD.

(D) RABV P does not block IFN induction in HEK293T cells expressing IRF3-5D. IFN induction was assessed using the luciferase assay. Cell lysates were analyzed using WB with anti-P and anti-tubulin antibodies. The bars represent the mean fold induction of firefly luciferase compared with unstimulated cells (not transfected with pIRF3-5D). EV, empty vector. Data points represent 3 independent experiments. Error bars indicate SD.

(E) Heatmap comparison of the abundance of proteins associated with P_{SAD} versus mutant P_{SAD}-S179P and control (CTRL), made with Qlucore AB version 3.7. Proteins (>2 unique peptides) were filtered on the basis of a multigroup comparison with $p < 0.005$. Abundance data were $\log_2$ transformed and standardized with a mean of 0 and variance of 1. A hierarchical clustering was applied on columns and rows were ordered according to principal-component analysis (PCA) component 1 from group comparison. Proteins in orange correspond to previously identified P partners. The heatmap is an active plot focused on proteins of higher abundance in P_{SAD} conditions versus the control.

(F) Co-immunoprecipitation of TBK1 with P from infected cells. N2A cells were infected with either SAD or SAD-S179P. Cells were treated with 300 μM of DSP before lysis and lysate immunoprecipitation with an anti-P antibody. Cell lysates (WCL) and immunoprecipitated proteins (IP) were analyzed using WB with anti-P and anti-TBK1 antibodies (R.S.I., relative signal intensity). The amount of TBK1 co-immunoprecipitated with P was quantified and normalized to the amount associated with P_{SAD} in 3 independent experiments. The mean is presented and error bars indicate SD. The experiment marked by a square was performed using 100 μM DSP.

(G) Interaction of inhibitory and non-inhibitory forms of P with hTBK1 assessed by Y2H system. Interaction between hTBK1 (or N_{CVS}) fused to Gal4-AD and different P fused to LexA-BD was assessed by yeast growth on His^- medium and the appearance of blue colonies in the presence of X-Gal. The line AD corresponds to Gal4-AD alone. Interaction of P with N_{CVS} was used as a positive control.

See also Figures S1 and S2.

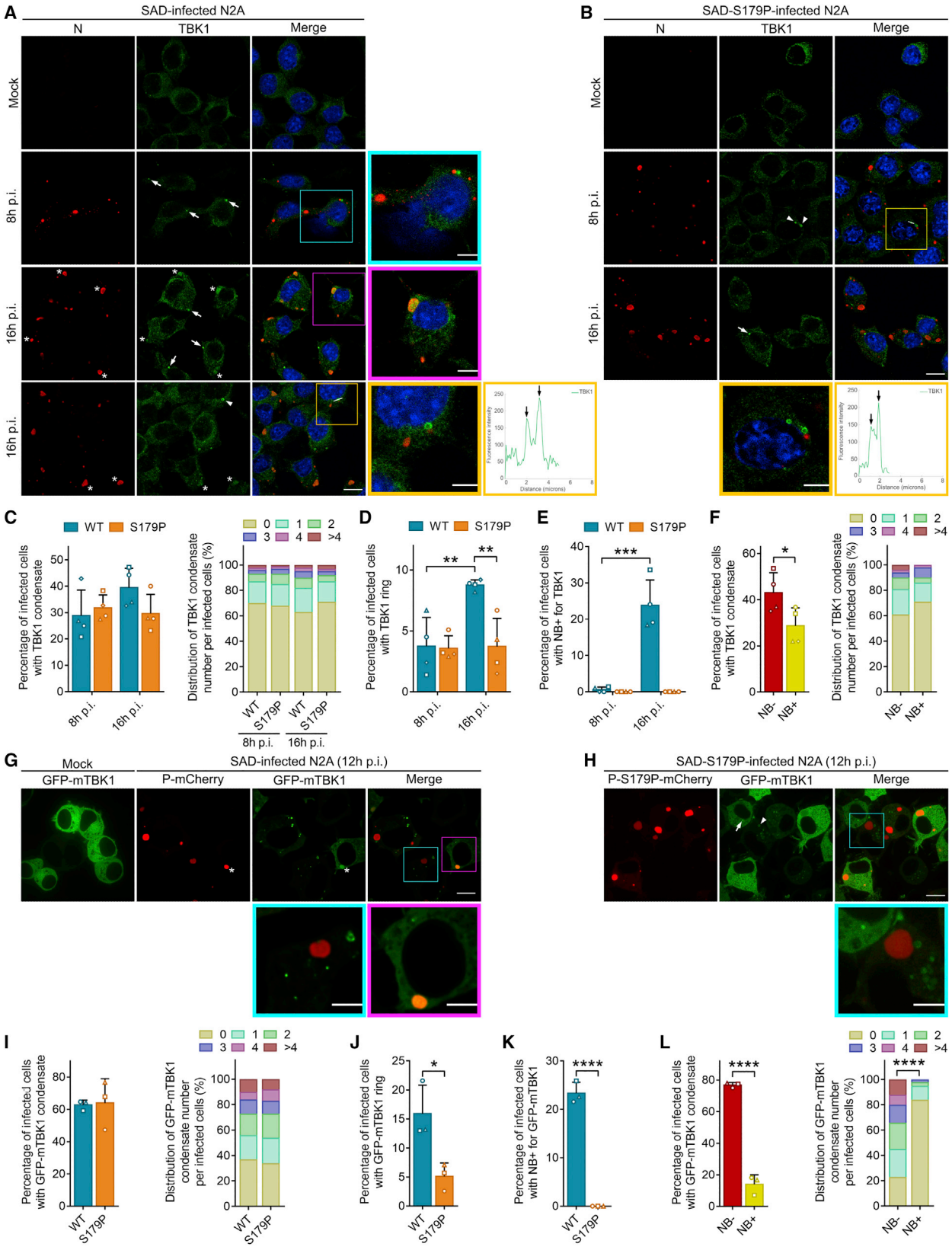

(legend on next page)

CellPress
OPEN ACCESS

whereas in SAD-S179P-infected cells, it translocates into the nucleus (Figure S1C). On the other hand, N2A infection with RABV did not lead to IFN-β induction (Figure S1B). These observations are consistent with the difference in infection phenotype of SAD-S179P in N2A and U-373MG cell lines (Figure S1A). In fact, SAD-S179P grows less efficiently than SAD in IFN-producing cells (U-373MG cells).

It has been shown that the inhibitory effect of P_{SAD} is due to its ability to prevent IRF3 phosphorylation.[27] Indeed, in HEK293T, when the IFN induction pathway was activated by a phosphomimetic version of IRF3 (IRF3-5D, containing mutations S396D, S398D, S402D, T404D, and S405D[35]) instead of ΔRIG-I, none of the P versions displayed any inhibitory effect (Figure 1D). This result confirmed that in the virus-induced signaling pathway, P_{SAD} targets a step upstream of IRF3 phosphorylation to exert its down-regulatory effect on IFN induction.[27]

TBK1 is associated with P-inhibitory forms

The difference in the inhibition activity of the two P proteins was an opportunity to identify the cellular protein(s), which once bound to P-inhibitory forms are unable to promote IRF3 activation.

To identify the cellular interactome of the different P proteins (P_{SAD} and P_{CVS} in their inhibitory and non-inhibitory forms), we co-transfected HEK293T cells with a plasmid encoding a C-terminal FLAG-tagged of each P protein (Figure S2A) and a plasmid encoding ΔRIG-I as IFN inducer. Protein complexes were immunoprecipitated using anti-FLAG-associated beads. The same amount of P was recovered for both wild-type (WT) and mutant P from the same viral strain (SAD or CVS) (Figures S2B and S2C). The protein complex composition was analyzed using protein mass spectrometry. Using quite stringent criteria for analysis (number of unique peptides identified > 2, $p < 0.005$), among previously identified P partners, HSP70[36] was found to be associated with all P forms, LC8[37] with both WT and mutant forms of P_{CVS}, and STAT1[28] and STAT2[29] with P_{SAD}-S179P (Figures 1E and S2D).

Interestingly, a single P partner, TBK1, was found to be preferentially associated with the inhibitory forms of P (Figures 1E and S2D). This interaction was validated by co-immunoprecipitation in N2A-infected cells using an anti-P antibody followed by TBK1 detection by western blot. In SAD-infected cells, the interaction between P and TBK1 was barely detected without cross-linking (Figure S2E) but much more visible after treatment with 3,3′dithiobis-(succinimidyl propionate) (DSP) (Figure 1F). In SAD-S179P-infected cells, the interaction appears much weaker with three times less TBK1 associated with the non-inhibitory P form. We also validated P-TBK1 interaction by the yeast two-hybrid (Y2H) system (Figure 1G). In this system, only P-inhibitory forms bind human TBK1 (hTBK1). As yeast is distant from mammalian cells, this indicates a direct P-TBK1 interaction not involving an intermediate protein.

TBK1 forms cytoplasmic inclusions and localizes in NBs formed by SAD

As TBK1 is one of the major kinases involved in IRF3 phosphorylation,[8,9] we decided to investigate its behavior during RABV infection.

Immunoblot analysis revealed that SAD or SAD-S179P infection has no significant impact on TBK1 expression level in N2A cells (Figure S2F). We then investigated the localization of TBK1 by immunofluorescence (IF). In mock-infected cells, we observed a faint and diffuse fluorescence in the cytoplasm (Figure 2A). By contrast, in SAD-infected N2A cells, as soon as 8 h p.i., we observed punctate TBK1 structures (further referred to as TBK1 condensates) that were distinct from NBs (Figures 2A and S3A). These condensates sometimes clustered to form ring-like structures (Figures 2A and S3E) that were found in 9%

Figure 2. TBK1 forms condensates and associates with NBs during RABV infection

(A and B) N2A cells were mock infected (mock), infected with SAD (A) or infected with SAD-S179P (B). At 8 or 16 h p.i., cells were fixed before analysis by confocal microscopy after co-staining with the mouse anti-N and rabbit anti-TBK1. Square boxes in the merge are magnified. TBK1 fluorescence (green) along the lines traced over a ring-like structure was quantified.

(C–F) Quantification of structures observed in (A) and (B) from cells infected for 8 or 16 h by SAD (n = 304 and n = 491 infected cells respectively from 4 independent experiments) or SAD-S179P (n = 353 and n = 470 infected cells respectively from 4 independent experiments).

(C) Percentage of infected cells containing TBK1 condensates (left panel) and distribution of the number of condensates per cell (right panel).

(D) Percentage of infected cells containing TBK1 ring-like structures.

(E) Percentage of infected cells with TBK1-containing NBs.

(F) Percentage of SAD-infected cells (16 h p.i.) with TBK1 condensates among cells presenting TBK1-containing NBs (i.e., NB+; n = 114 cells) or not (i.e., NB−; n = 377 cells) (left panel) and distribution of the number of condensates per cell in cells presenting TBK1-containing NBs (NB+) or not (NB−) (right panel).

(G) N2A cells were mock infected or infected with SAD and transfected with both pP_{SAD}-mCherry and pGFP-mTBK1. At 12 h p.i., live cells were analyzed using confocal spinning disk microscopy. Square boxes in the merge are magnified.

(H) N2A cells were infected with RABV SAD-S179P and transfected with both pP-S179P-mCherry (to visualize NBs) and pGFP-mTBK1, and analyzed as in (G). Square box in the merge is magnified.

(I–L) Quantification of structures observed in (G) and (H) from cells infected for 12 h by SAD (n = 158 infected and transfected cells from 3 independent experiments) or SAD-S179P (n = 147 infected and transfected cells from 3 independent experiments).

(I) Percentage of infected cells containing GFP-mTBK1 condensates (left panel) and distribution of the number of condensates per cell (right panel).

(J) Percentage of infected cells containing GFP-mTBK1 ring-like structures.

(K) Percentage of infected cells with GFP-mTBK1-containing NBs.

(L) Percentage of SAD-infected cells (16 h p.i.) with GFP-mTBK1 condensates among cells presenting GFP-mTBK1-containing NBs (i.e., NB+; n = 37 cells) or not (i.e., NB−; n = 121 cells) (left panel) and distribution of the number of condensates per cell in cells presenting GFP-mTBK1-containing NBs (NB+) or not (NB−).

Arrows, TBK1 condensates; arrowheads, TBK1 ring-like structures; asterisks, TBK1-containing NBs. Scale bar: 10 μm, except in magnified images (scale bar: 5 μm). The bars represent the mean ± SD. Data points represent replicates of three independent experiments. Significant differences are indicated (*$p < 0.05$, **$p < 0.01$, ***$p < 0.001$, and ****$p < 0.0001$) after application of Student's t test (for percentage analysis) or the Kolmogorov-Smirnov test (for distribution analysis). See also Figure S3.

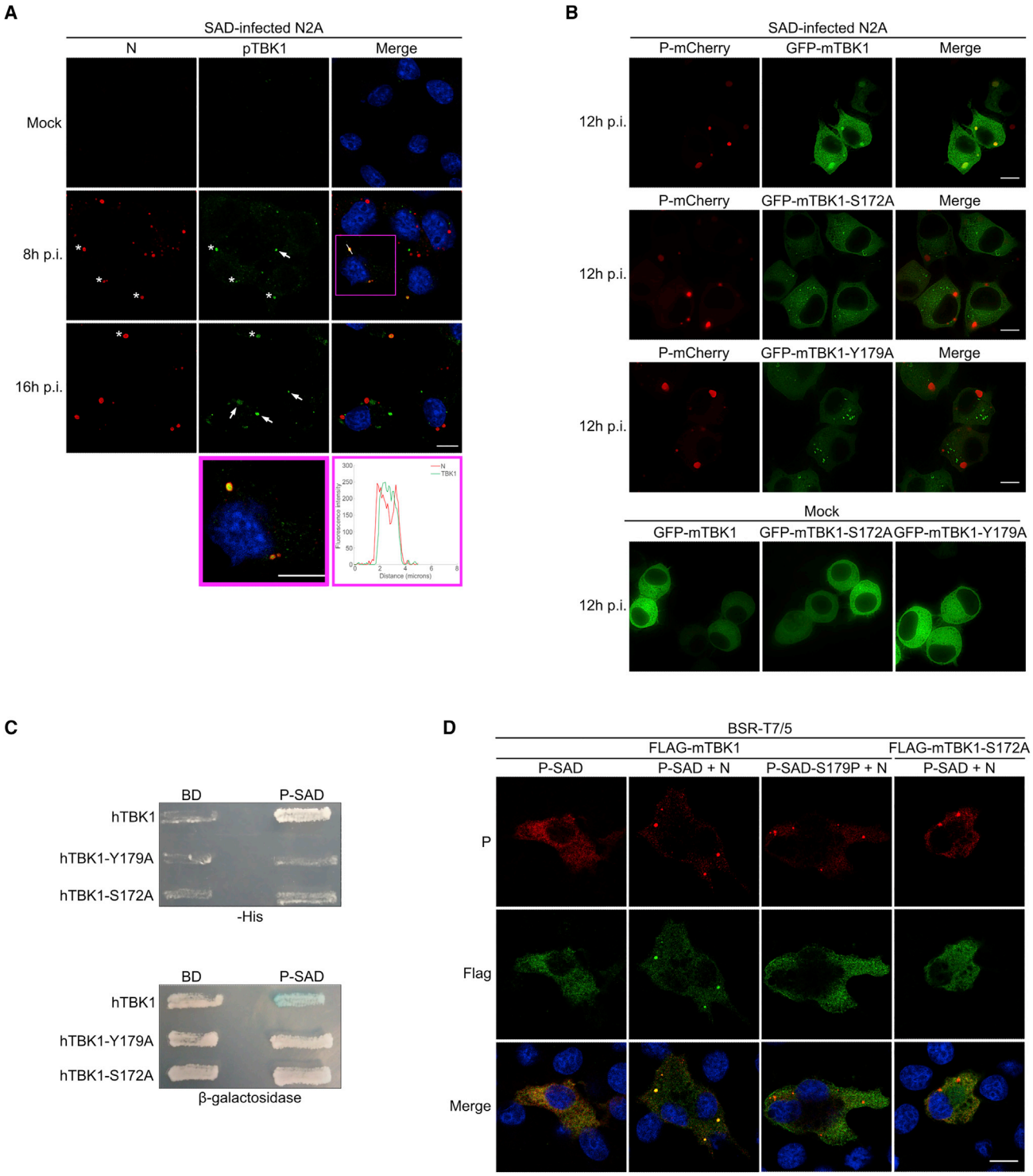

Figure 3. TBK1 phosphorylation is required for association with NBs

(A) Phosphorylated TBK1 colocalize with NBs. N2A cells were mock infected (mock) or infected with SAD. At 8 or 16 h p.i., cells were fixed before analysis by confocal microscopy after co-staining with the mouse anti-N and rabbit anti-pTBK1(S172). Square box in the merge is magnified. The fluorescence corresponding to TBK1 (green) and N (red) along the line traced over an NB has been quantified. Arrows indicate TBK1 condensates, and asterisks indicate TBK1-containing NBs.

(B) TBK1 phosphorylation mutants do not colocalize with NBs. N2A cells were mock infected (mock) or infected with SAD and transfected with pP_{SAD}-mCherry and either pGFP-mTBK1 or pGFP-mTBK1-S172A or pGFP-mTBK1-Y179A. At 12 h p.i., live cells were analyzed using epifluorescence microscopy.

(legend continued on next page)

of the cells at 16 h p.i. (Figure 2D). At 16 h p.i., TBK1 was also found to be associated with NBs formed by SAD (Figures 2A, 2E, and S3A). Of note, infected cells, in which TBK1 was associated with NBs, contained fewer condensates (Figure 2F). Importantly, cell fixation was critical for the observation of TBK1 condensates and TBK1 association with NBs. Indeed, these features were detected when the cells were fixed with methanol/acetone but not with paraformaldehyde (PFA) (Figures S3A and S3B).

To ensure that these condensates did not result from a sample preparation artifact, we decided to perform live imaging using plasmids encoding a fluorescent GFP-TBK1. Of note, GFP-hTBK1 was as efficient as TBK1 for IFN induction (Figure S3F). TBK1 condensates and TBK1 concentration in NBs were observed by live imaging of SAD-infected N2A cells transfected with two plasmids allowing the expression of a fluorescent version of murine TBK1 (GFP-mTBK1) and a fluorescent version of P_{SAD} (P_{SAD}-mCherry) to visualize NBs (Figure 2G). Again, GFP-mTBK1 condensates were not observed in absence of infection (Figure 2G, mock) indicating that the viral infection triggered their formation. Upon PFA fixation, GFP-mTBK1 condensates were still observed by GFP fluorescence, but not when using an anti-TBK1 antibody (Figures S3C and S3D). This suggests that in PFA-fixed cells, TBK1, when in condensates or in NBs, is not accessible or recognized by the antibody. Finally, when GFP-mTBK1 was found to be associated with NBs, less GFP-mTBK1 condensates were observed (Figure 2L; Videos S1 and S2). Only 16% of the N2A cells, in which GFP-mTBK1 was found to be associated with NBs, contain GFP-mTBK1 condensates instead of 77% in absence of association of GFP-mTBK1 with the viral factory (Figure 2L).

TBK1 condensates were also detected in N2A cells infected with SAD-S179P or CVS (i.e., expressing a non-inhibitory form of P) and fixed with methanol/acetone (Figures 2B and S3G). The percentage of infected cells containing condensates and the distribution of the number of condensates per cell was similar for both SAD and SAD-S179P (Figure 2C). The two major differences were (1) the lack of TBK1 association with NBs formed in SAD-S179P-infected cells (Figure 2E) and (2) a smaller proportion of ring-like structures at 16 h p.i. in SAD-S179P-infected cells (Figure 2D). These observations were confirmed by live imaging on SAD-S179P-infected N2A cells, transfected with GFP-mTBK1 (Figures 2H–2K).

Taken together, these data indicate that in N2A cells, RABV infection induces TBK1 condensate formation and that TBK1 is partly concentrated in NBs formed by SAD (but not by SAD-S179P).

TBK1 phosphorylation is required for P_{SAD} binding

As TBK1 is phosphorylated upon viral detection by the sensors of the innate immune system, we performed IF using antibody anti-pTBK1(S172). No fluorescence was observed in mock-infected cells except in dividing cells as already described (Figure S4A).[38] In SAD-infected N2A cells, pTBK1 was detected in NBs and in cytoplasmic condensates (Figure 3A). Cytoplasmic condensates containing pTBK1 were observed as early as 8 h p.i. in U-373MG cells (Figure S4B). Of note, in U-373MG cells, there was no association of pTBK1 with NBs. Nevertheless, at 16 h p.i., fewer TBK1 condensates were observed in cells infected with SAD compared with SAD-S179P. This was the consequence of an increase in the proportion of SAD-S179P-infected cells containing TBK1 condensates at 16 h p.i. compared with 8 h p.i. (Figure S4C). Thus, in this cell line, condensate formation precedes IFN-β induction and more condensates are detected with the virus unable to inhibit IFN production (Figure S1B).

To evaluate the effect of TBK1 phosphorylation, we overexpressed fluorescent versions of phosphorylation mutants of TBK1 in N2A-infected cells. The first mutant was GFP-mTBK1-S172A that is unable to be phosphorylated at position 172.[39–41] The second was GFP-mTBK1-Y179A, as phosphorylation of tyrosine 179 is required for subsequent autophosphorylation of TBK1 at serine 172.[42] Both phosphorylation mutants failed to accumulate in NBs indicating that TBK1 phosphorylation is required for TBK1 recruitment to the viral factories. Nevertheless, both mutants still formed condensates in infected cells (Figure 3B).

As TBK1 phosphorylation mutants were not recruited into NBs, we investigated their interactions with P using the Y2H system. Both hTBK1-S172A and hTBK1-Y179A failed to interact with P_{SAD} (Figure 3C). As overexpression of hTBK1 in yeast, but not that of the phosphorylation mutants, promotes its phosphorylation (Figure S4D) (probably by homodimerization and intermolecular transphosphorylation), the lack of interaction with the phosphorylation mutants suggests that TBK1 autophosphorylation is required for P_{SAD} binding.

The localization of TBK1 in N-P inclusions depends on P ability to inhibit IFN production

We have previously developed a minimal system recapitulating NB properties using BSR cells constitutively expressing the T7 RNA polymerase (BSR-T7/5).[19] When those cells are co-transfected with plasmids pTit-P and pTit-N, cytoplasmic spherical inclusions are formed that have the same liquid properties as NBs.[19] We co-transfected BSR-T7/5 cells with plasmids pTit-P, PTit-N, and pTit-FLAG-mTBK1. P and N were from either the SAD strain (Figure 3D) or the CVS strain (Figure S4E). For each strain, we used both the IFN inhibitory (P_{SAD} and P_{CVS}-P179S) or non-inhibitory (P_{SAD}-S179P and P_{CVS}) version of P. FLAG-mTBK1 was found to be associated with the N-P inclusions if and only if the inhibitory version of P, which binds TBK1, was expressed (Figures 3D for SAD and S4E for CVS).

(C) Interaction of P_{SAD} with hTBK1 and its phosphorylation mutants assessed by Y2H system. The interactions between TBK1 (WT or phosphorylation mutants) fused to Gal4-AD and different P forms fused to LexA-BD were assessed by yeast ability to grow on His-medium and the appearance of blue colonies in the presence of X-Gal. The line BD corresponds to LexA-BD alone.

(D) Association of TBK1 with inclusion bodies formed in the cellular minimal system. BSR-T7/5 cells were co-transfected with plasmids pTit-P_{SAD} or pTit-P_{SAD}-S179P, pTit-N, and pTit-FLAG-mTBK1 or pTit-FLAG-mTBK1-S172A. After 24h, cells were fixed and analyzed using confocal microscopy after co-staining with the rabbit anti-P and mouse anti-FLAG.

Scale bars: 10 μm. See also Figure S4.

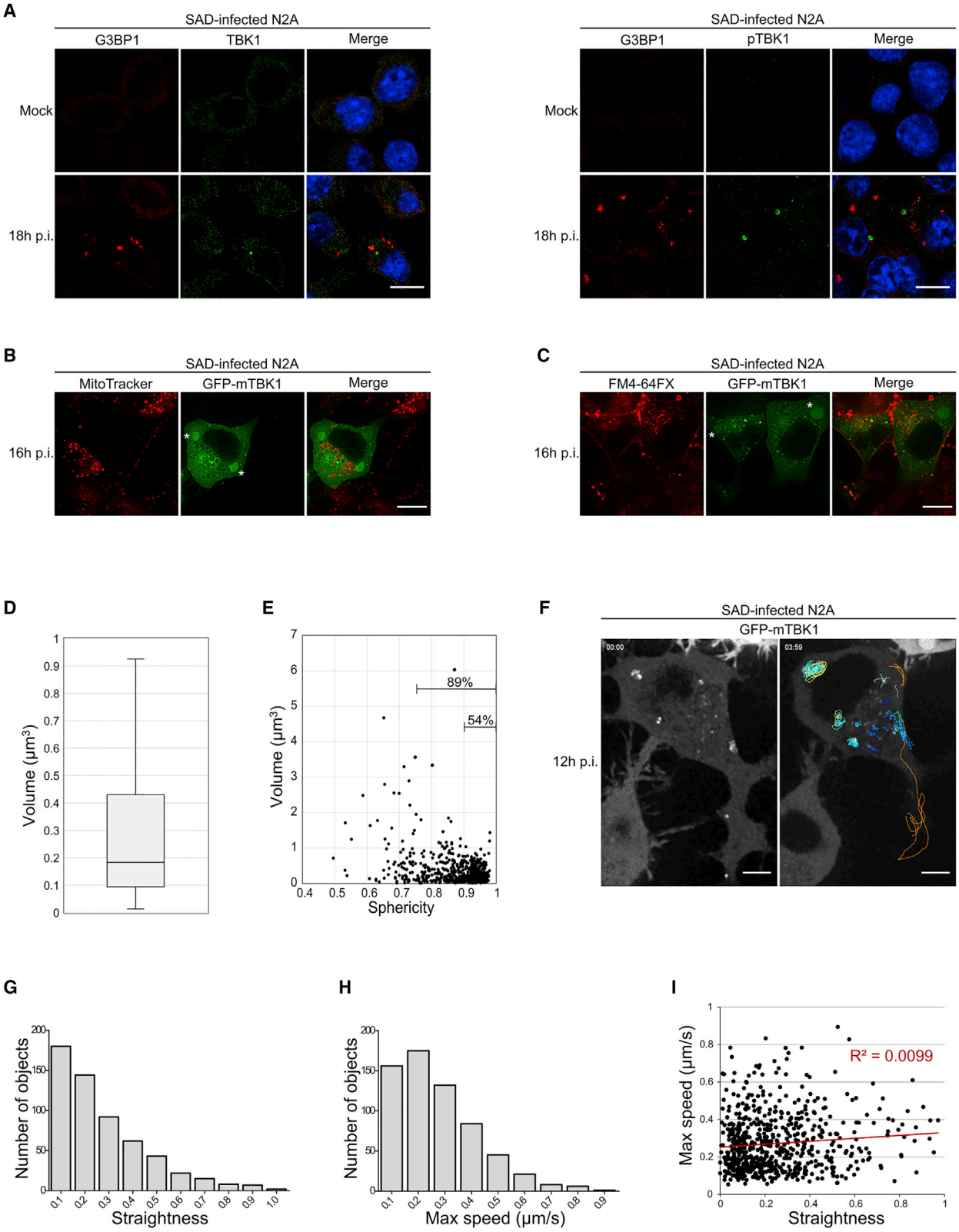

(legend on next page)

CellPress
OPEN ACCESS

This localization was also dependent on TBK1 phosphorylation as mTBK1-S172A failed to associate with N-P inclusions (Figures 3D and S4E).

Characterization of TBK1 condensates and their dynamics

As RABV infection induces the formation of stress granules (SGs) in U-373MG and N2A cell lines,[43] we wondered if TBK1 condensates colocalized with such structures. We analyzed the localization of SGs in N2A-infected cells using an antibody directed against G3BP1, a central component of SGs.[44] There was no colocalization of endogenous TBK1 condensates with SGs (Figure 4A). Similarly, no colocalization of GFP-mTBK1 condensates with MitoTracker-labeled mitochondria was observed (Figure 4B). Finally, we used FM4-64FX, a dye known to label cellular membranes. This marker was not associated with GFP-mTBK1 condensates (Figure 4C). These data indicated that TBK1 condensates are distinct from previously described cellular organelles.

In infected cells, observed after fixation or by live imaging, TBK1 condensates appear to be rather spherical. This was quantified in cells infected with SAD and transfected with pGFP-mTBK1 using live imaging and three-dimensional (3D) reconstruction (Figure 4D). TBK1 condensates had a median volume of 0.183 μm^3 (corresponding to a diameter of 0.704 μm for a sphere). Globally, 54% (respectively 89%) of them have a sphericity greater than 0.9 (respectively 0.75) (Figure 4E). Their sphericity decreases when object gets bigger (Figure 4E). Those bigger objects appear less regular (Video S1), often forming heterogeneous ring-like structures (Video S3), with a grainy appearance (see also the micrographs gallery in Figure S3E). This suggests that they result from the self-association of smaller condensates.

In live imaging, we observed that TBK1 condensates were moving inside the cytoplasm. Analysis of their trajectories revealed two kinds of behavior: the vast majority displayed locally restricted movement, while a few moved across the cell with rather straight trajectories (Figures 4F and 4G; Videos S4 and S5). Locally restricted circumvolutions were observed when TBK1 condensates self-associate to form large and irregular objects. However, the maximum speed of the condensates did not depend on the nature of their trajectories (i.e., whether it was straight of circumvoluted) (Figures 4H and 4I).

Localization of proteins NAP1 and SINTBAD in RABV-infected cells

Effective signal transduction upon viral infection requires TBK1 association with proteins such as NAP1, SINTBAD, TANK, TRIF, or OPTN.[14,15,45–48] We therefore analyzed the localization of these proteins. For both NAP1 and SINTBAD (Figures 5A and 5B), the infection of cells (either by SAD or SAD-S179P) induced the formation of cytoplasmic condensates, absent in mock-infected cells, which sometimes adopt ring-like structures for NAP1. These proteins were also weakly associated with NBs when cells were infected with SAD but not when infected with SAD-S179P. The localization of TRIF (involved in the TLR3 pathway) and OPTN (involved in autophagy) is not affected by infection (Figure S5). Indeed, in mock-infected cells as well as in SAD- and SAD-S179P-infected cells, OPTN exhibits its typical Golgi apparatus localization[49] (Figure S5A), while TRIF remains diffuse in the cytoplasm (Figure S5B). Finally, we were unable to characterize the localization of TANK using a commercial antibody.

To exclude artifacts linked to cell fixation, we also analyzed the localization of SINTBAD and NAP1 in live cells. For this, N2A cells were transfected with plasmids encoding a protein amino-terminally fused to either mCherry or GFP (mCherry-mNAP1, GFP-mNAP1, mCherry-mSINTBAD and GFP-mSINTBAD). Expression of the fluorescent versions of NAP1 or SINTBAD induces the formation of condensates like those observed in fixed cells after infection (Figure 5C). This indicates that infection as well as NAP1 or SINTBAD overexpression triggers condensate formation.

When the cells were infected with SAD and subsequently co-transfected with two plasmids (P_{SAD}-mCherry and GFP-mNAP1 or GFP-mSINTBAD), cytoplasmic condensates of NAP1 or SINTBAD were formed but did not colocalize with NBs (Figure 5D).

We also co-transfected N2A cells with pGFP-mTBK1 and a plasmid allowing the expression of NAP1 or SINTBAD fused to mCherry. Co-expression of GFP-mTBK1 and mCherry-mNAP1 in non-infected cells induced the formation of condensates of

Figure 4. Characterization of TBK1 condensates

(A) TBK1 condensates are distinct from stress granules. N2A cells were mock infected (mock) or infected with SAD. At 18 h p.i., cells were fixed before analysis by confocal microscopy after co-staining with the mouse anti-G3BP1 and either rabbit anti-TBK1 (left panel) or rabbit anti-pTBK1(S172) (right panel).

(B) TBK1 condensates are distinct from mitochondria. N2A cells were infected with SAD and transfected with pGFP-mTBK1. At 15 h p.i., cells were incubated with MitoTracker. After 1 h, live cells were analyzed using epifluorescence microscopy.

(C) TBK1 condensates are not labeled by the lipophilic probe FM4-64FX. N2A cells were infected with SAD and transfected with pGFP-mTBK1. At 12 h p.i., cells were incubated with FM4-64FX for 4 h before analysis by live epifluorescence microscopy.

In (B) and (C), asterisks indicate GFP-mTBK1-containing NBs. In (A), (B), and (C), scale bar: 10 μm.

(D and E) Characterization of GFP-mTBK1 condensates size and shape. Boxplot representing the volume distribution of the GFP-mTBK1 condensates (D) and dot plot representing the relation between the volume and the sphericity of GFP-mTBK1 condensates (E) in N2A cells infected with SAD and transfected with pGFP-mTBK1 (observation 12 h. p.i.; 39 cells, 700 particles).

(F) Characterization of GFP-mTBK1 condensates dynamics in infected cells. GFP-mTBK1 condensates tracking experiments in N2A cells infected with SAD and transfected with pGFP-mTBK1 and pP-mCherry (spinning disk observation, 12 h p.i.). The micrograph on the left indicates the cellular initial state. Trajectories are traced on the right image (Videos S4 and S5). Scale bar: 5 μm.

(G) Histogram showing the distribution of trajectory straightness of GFP-mTBK1 condensates.

(H) Histogram showing the distribution of maximal speed of GFP-mTBK1 condensates along their trajectory.

(I) Dot plot highlighting the absence of relation between the particle maximal speed and the straightness of the trajectory.

Data presented in (G), (H), and (I) are derived from 628 trajectories extracted from 14 cells.

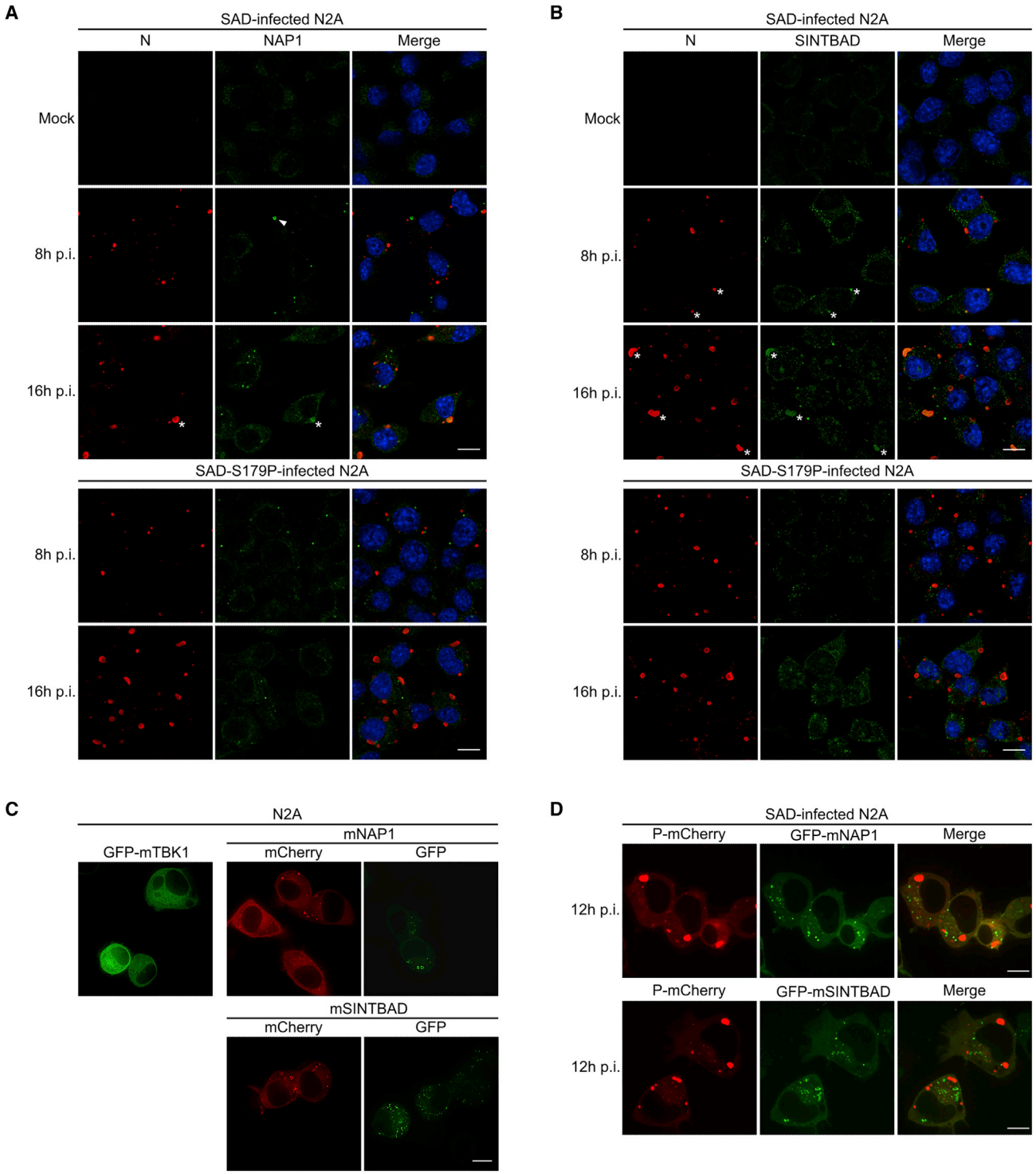

Figure 5. Localization of NAP1 and SINTBAD in RABV-infected N2A cells

(A and B) N2A cells were mock infected (mock) or infected with indicated virus. At 8 or 16 h p.i., cells were analyzed using confocal microscopy after co-staining with the mouse anti-N and rabbit anti-NAP1 (A) or anti-SINTBAD (B). Asterisks, NAP1/SINTBAD-containing NBs; arrowhead, NAP1 ring-like structure.

(C) Fluorescent versions of mNAP1 and mSINTBAD form condensates. N2A cells were either transfected with pGFP-mTBK1, pmCherry-mNAP1, pGFP-mNAP1, pmCherry-mSINTBAD, or pGFP-mSINTBAD. After 18 h, live cells were analyzed using epifluorescence microscopy.

(D) GFP-mNAP1 and GFP-mSINTBAD do not associate with NBs. N2A cells were infected with SAD and transfected with pP_{SAD}-mCherry together with pGFP-mNAP1 or pGFP-mSINTBAD. At 12 h p.i., live cells were analyzed using confocal spinning disk microscopy.

Scale bar: 10 μm. See also Figure S5.

CellPress
OPEN ACCESS

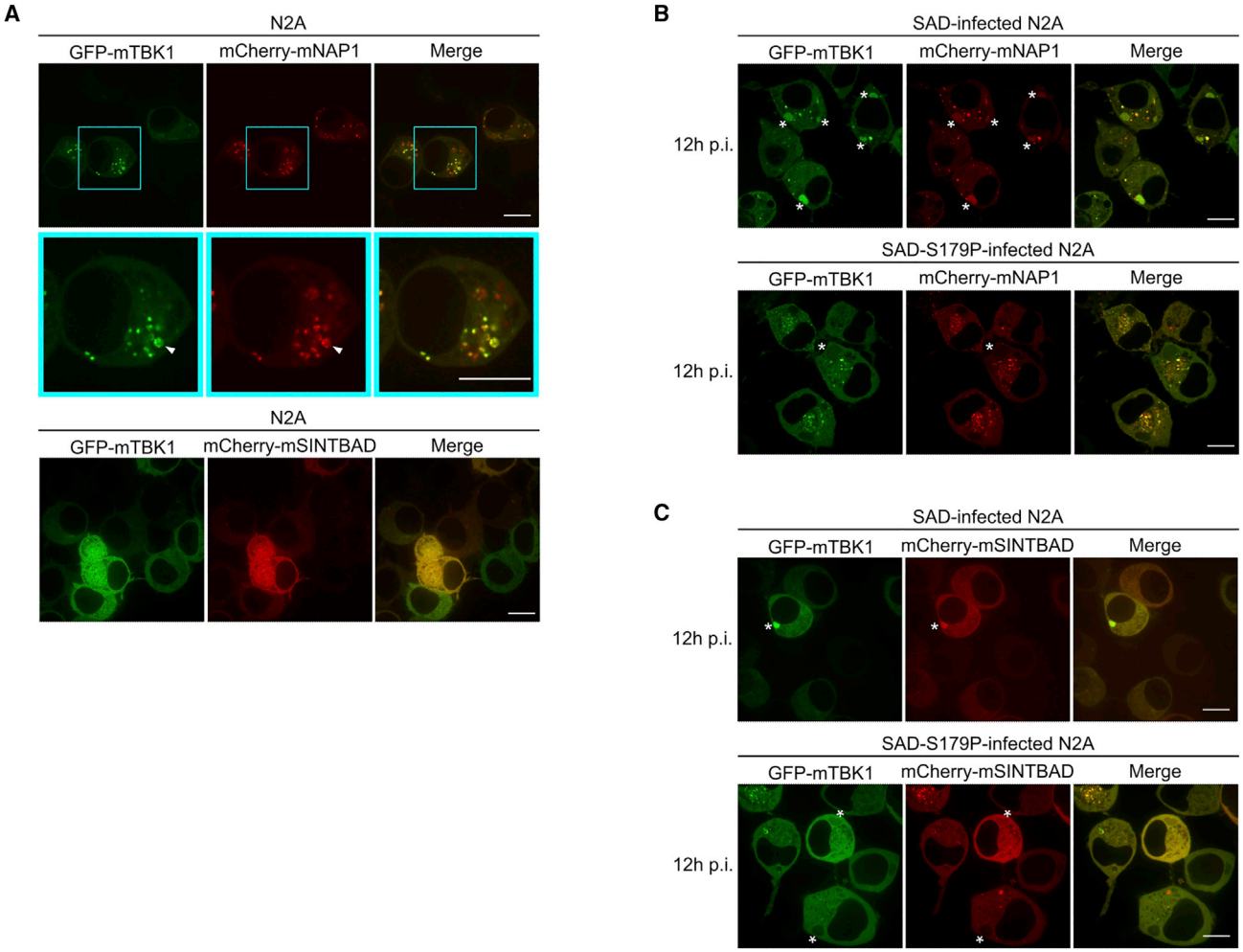

Figure 6. Co-expression of TBK1 and its partners influences their localization

(A) N2A were transfected with pGFP-mTBK1 and either pmCherry-mNAP1 or pmCherry-mSINTBAD. After 18 h, live cells were analyzed using confocal spinning disk microscopy. Arrowhead, ring-like structure.

(B and C) N2A were infected with the indicated virus and transfected with pGFP-mTBK1 as well as with pmCherry-mNAP1 (B) or pmCherry-mSINTBAD (C). At 12 h p.i., live cells were analyzed using confocal spinning disk microscopy. Asterisks indicate NBs (which appear in negative contrast when TBK1 is excluded from them in cells infected with SAD-S179P).

Scale bars: 10 μm.

both proteins that often colocalized including in the previously described ring-like structures (Figure 6A). This was in contrast with the absence of condensates in cells co-expressing GFP-mTBK1 and mCherry-mSINTBAD (Figure 6A). This suggested that NAP1 is a positive regulator of TBK1 condensate formation, whereas TBK1 is a negative regulator of SINTBAD condensate formation.

When cells were infected with SAD and then co-transfected with pGFP-mTBK1 and pmCherry-mNAP1, condensates of the two proteins were observed (Figure 6B). As expected, GFP-mTBK1 was found to be associated with NBs (that were detected because of their intense GFP fluorescence). In contrast to the results of Figure 5D, in which TBK1 was not overexpressed, mCherry-mNAP1 was found to be associated with NBs. In SAD-S179P-infected cells, neither GFP-mTBK1 nor mCherry-mNAP1 was found to be associated with NBs (that were then detected in negative on a green GFP background) (Figure 6B). Therefore, TBK1 overexpression drives TBK1-NAP1 complex localization in NBs containing the inhibitory form of P.

A similar observation was made in infected cells after co-expression of GFP-mTBK1 and mCherry-mSINTBAD. Both GFP-mTBK1 and mCherry-mSINTBAD were found to be associated with NBs in SAD-infected cells but not in SAD-S179P-infected cells (Figure 6C). Here again, TBK1 overexpression drives TBK1-SINTBAD complex localization in NBs containing the inhibitory form of P. Of note, the overexpression of both GFP-mTBK1 and mCherry-mSINTBAD drastically reduced the number of condensates of both proteins in infected cells (Figure 6C). Nevertheless, in the rare cells in which both GFP-mTBK1 and

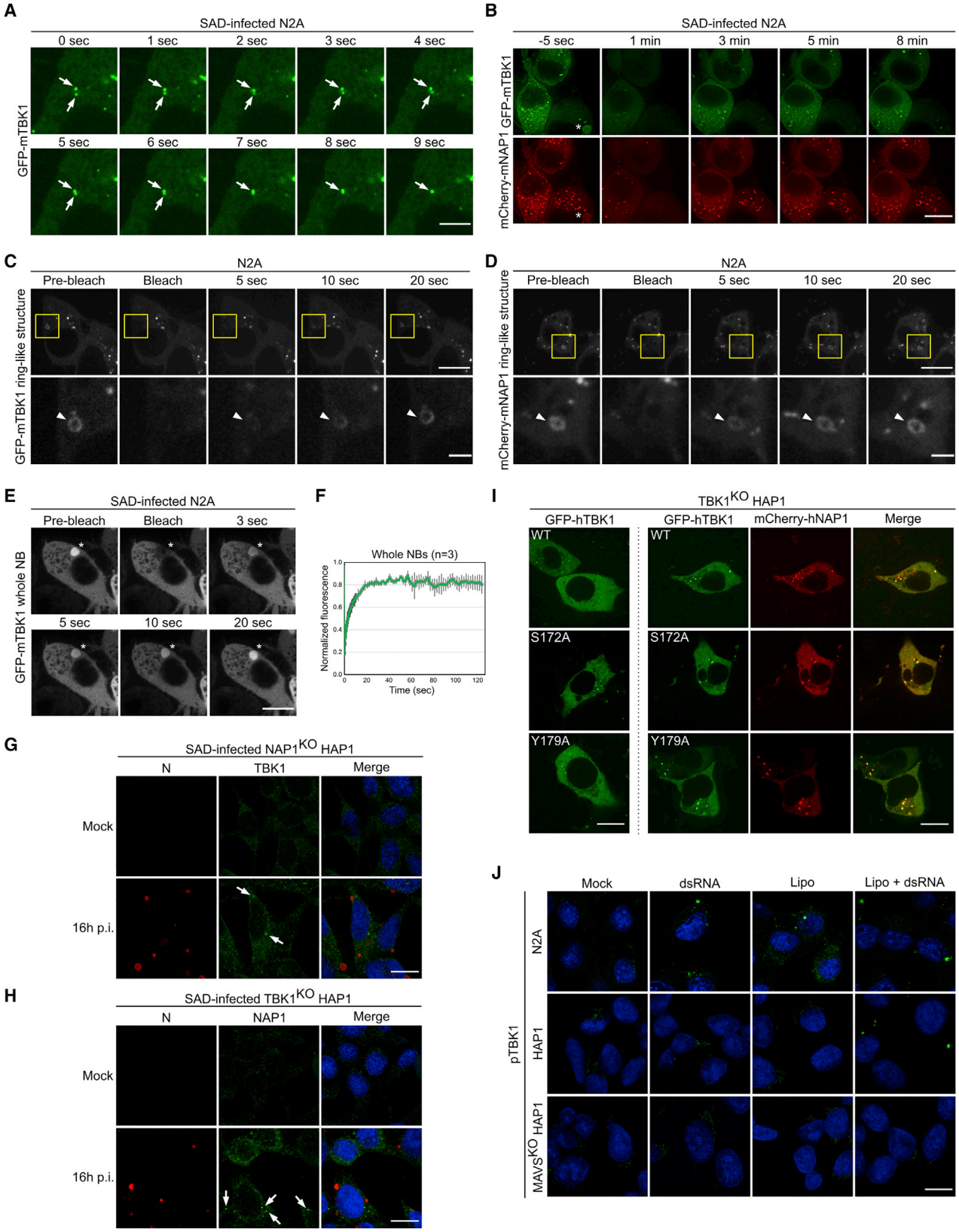

(legend on next page)

CellPress
OPEN ACCESS

mCherry-mSINTBAD condensates were present, colocalization was observed (e.g., SAD-S179P-infected cell, upper left corner of Figure 6C).

Condensates formed by TBK1 and NAP1 have liquid properties

We characterized NAP1 condensates in cells infected with SAD and transfected with pmCherry-mNAP1 using live imaging and 3D reconstruction (Figures S6A and S6B). mCherry-mNAP1 condensates had a median volume of 0.302 μm^3 (corresponding to a diameter of 0.832 μm for a sphere) (Figure S6A). Globally, 60% (respectively 92%) of them have a sphericity greater than 0.9 (respectively 0.75) (Figure S6B).

The spherical aspect of TBK1 (Figure 4E) and NAP1 condensates (Figure S6B) as well as the fact that TBK1 condensates are apparently devoid of membranes (Figure 4C) suggested that these proteins form liquid condensates. Consistently, we observed some fusion events between GFP-mTBK1 condensates (Figure 7A; Video S6). However, the small size of the condensates and their dynamics make difficult the visualization of such events.

Several liquid condensates formed by LLPS are sensitive to cellular hypotonic shock.[19,50,51] We investigated the behavior of GFP-mTBK1 and mCherry-mNAP1 condensates upon such a treatment. SAD-infected N2A cells, transfected with plasmids pGFP-mTBK1 and pmCherry-mNAP1, were incubated with DMEM medium diluted 5 times in water. This hypotonic shock resulted in a fast and complete disappearance of NBs, as already described,[19] as well as that of TBK1 condensates, while NAP1 condensates were only partially sensitive to this treatment (Figure 7B; Video S7). The condensate disappearance was followed by their reformation within 3 min.

Finally, we performed fluorescence recovery after photobleaching (FRAP) experiments in N2A cells co-transfected with pGFP-mTBK1 and pmCherry-mNAP1. We photobleached both GFP-mTBK1 and mCherry-mNAP1-containing ring-like structures. Although the whole structure was photobleached, the recovery of fluorescence signal was quite fast (Figures 7C and 7D). This indicated that TBK1 and NAP1 shuttle between their cytoplasmic pool and the condensates. Taken together, all the experimental data are consistent with a liquid nature of the condensates formed by TBK1 and NAP1.

We also analyzed the nature of the interaction between TBK1 and the NBs formed in SAD-infected N2A cells. FRAP experiments performed on GFP-mTBK1 concentrated in NBs (Figures 7E and S6C) revealed a fast recovery with a half-time of about 5 s (Figure 7F) that is very similar to the one of P-mCherry protein, when photobleached in the same structures.[19] Therefore, TBK1, like P, behaves in NBs as in a liquid environment.

TBK1 and NAP1 form condensates independently of each other

We then investigated the behavior of NAP1 in TBK1-deficient HAP1 cells (TBK1^{KO} HAP1) (Figure S7C) and that of TBK1 in NAP1-deficient HAP1 cells (NAP1^{KO} HAP1) (Figure S7C). As in N2A, in the control parental HAP1 cell line, we observed condensates for both proteins upon RABV infection (Figures S7A and S7B). These condensates were absent in mock-infected cells. In NAP1^{KO} cells (respectively in TBK1^{KO} cells), TBK1 (respectively NAP1) formed condensates upon RABV infection (Figures 7G and 7H). Therefore, both proteins form condensates independently of each other.

Finally, co-expression of GFP-hTBK1 (or mutants GFP-hTBK1-S172A and GFP-hTBK1-Y179A) and mCherry-hNAP1 induces similar condensates of both proteins in HAP1 parental cell line (Figure S7D) as in TBK1^{KO} HAP1 cells (Figure 7I). This indicates that the formation of TBK1 condensates by the mutant forms is not due to their recruitment in preformed endogenous TBK1 condensate. Therefore, neither the phosphorylation of TBK1 in position 172 nor in position 179 is required for TBK1 condensate formation.

Figure 7. TBK1 and NAP1 condensates have liquid properties

(A) Fusion between GFP-mTBK1 condensates. N2A cells were infected with SAD and transfected with pGFP-mTBK1 and pmCherry-mNAP1. At 12 h p.i., live cells were analyzed using confocal spinning disk microscopy. Images are from Video S5. Scale bar: 5 μm.

(B) GFP-mTBK1 and mCherry-mNAP1 condensates are sensitive to a hypotonic shock. N2A cells were infected with SAD and transfected with pGFP-mTBK1 and pmCherry-mNAP1. At 14 h p.i., a hypotonic shock was applied. Images are from Video S6 at indicated time pre- and post-shock. Scale bar: 10 μm.

(C and D) FRAP on ring-like structures formed by GFP-mTBK1 (C) and mCherry-mNAP1 (D) in N2A co-transfected cells (18 h). The diameter of the photobleached region was 1.4 μm. Scale bars: 2 μm (lower rows), 10 μm (upper rows).

(E and F) FRAP on GFP-mTBK1 located inside NB. Whole NBs were photobleached. N2A cells were infected with SAD and transfected with pGFP-mTBK1 and pP-mCherry. FRAP experiments were performed 12 h p.i. The diameter of the photobleached region was of 2.8 μm. Scale bar: 10 μm. In (F), the mean of 3 FRAP experiments is shown in green. Error bars represent the SD.

(G) SAD infection induces TBK1 condensate formation independently of NAP1. NAP1^{KO} HAP1 were mock infected (mock) or infected with SAD. At 16 h p.i., cells were fixed before analysis by confocal microscopy after co-staining with the mouse anti-N and rabbit anti-TBK1. Scale bar: 10μm. Arrows indicate TBK1 condensates.

(H) SAD infection induces NAP1 condensate formation independently of TBK1. TBK1^{KO} HAP1 were mock infected (mock) or infected with SAD. At 16 h p.i., cells were fixed before analysis by confocal microscopy after co-staining with the mouse anti-N and rabbit anti-NAP1. Scale bar: 10 μm. Arrows indicate NAP1 condensates.

(I) GFP-hTBK1 phosphorylation mutants form condensates independently of endogenous TBK1. TBK1^{KO} HAP1 were transfected either with pGFP-hTBK1-WT, or pGFP-hTBK1-S172A, or pGFP-hTBK1-Y179A (left panels) and co-transfected with pmCherry-hNAP1 (right panels). After 18 h, live cells were analyzed using confocal spinning disk microscopy. Scale bar: 10 μm.

(J) Formation of TBK1 condensates upon cell exposure to danger signals. N2A, control parental HAP1, and MAVS^{KO} HAP1 cells were either mock-treated (Mock) (i.e., incubated with the medium without dsRNA or lipofectamine 3000), incubated with medium containing 4 μg/ml 5′ppp-dsRNA (dsRNA), incubated with medium containing lipofectamine 3000 alone (Lipo), or transfected with 5′ppp-dsRNA using lipofectamine 3000 (Lipo + dsRNA). After 6h, cells were fixed before staining with the rabbit anti-pTBK1(S172) and analysis by confocal microscopy. The scale bar corresponds to 10 μm.

See also Figures S6 and S7.

Both cytosolic and extracellular dsRNA induce TBK1 condensate formation

TBK1 is activated when PRRs sense dsRNA. To investigate if the presence of dsRNA could trigger TBK1 condensate formation, N2A cells were either incubated or transfected with 5′ppp-dsRNA before fixation after 6h. Endogenous phosphorylated TBK1 protein was analyzed using the anti-pTBK1(S172) antibody (Figures 7J and S7E).

Incubation with 5′ppp-dsRNA induced the formation of TBK1 condensates that often assembled into rings (Figures 7J and S7E). Such condensates were not observed in mock-treated N2A cells. This indicated that extracellular dsRNA is a danger signal that induces TBK1 condensate formation, most probably by the TLR3 pathway.

As TBK1 condensates were also detected in control N2A cells that were treated with lipofectamine only (i.e., without 5′ppp-dsRNA) (Figures 7J and S7E), it was not possible to conclude as to the formation of condensates upon IFN induction by cytosolic PRRs in this cell line.

We then performed the same experiments on HAP1 cells, known not to express TLR3.[52] As expected, incubation with 5′ppp-dsRNA did not induce the formation of TBK1 condensates (Figure 7J). Interestingly, TBK1 condensates were observed in HAP1 cells transfected with 5′ppp-dsRNA using lipofectamine but not in control cells incubated with lipofectamine alone (Figure 7J). This suggested that TBK1 condensates were also formed upon cytosolic PRR signaling. This was verified using MAVS-deficient HAP1 cells (MAVS^{KO} HAP1) (Figure S7C). Indeed, in this cell line, no TBK1 condensates were observed upon cell transfection with 5′ppp-dsRNA (Figure 7J), nor upon RABV infection (Figure S7F).

Taken together, the data indicate that both extracellular and cytosolic 5′ppp-dsRNA constitute danger signals that induce TBK1 condensate formation through TLR3-and RIG-I/MDA-5-dependent signaling leading to IFN induction. They also reveal that lipofectamine alone also triggers the IFN induction pathway in N2A cells in agreement with previous observations in some other cell lines.[53,54]

DISCUSSION

The recent discovery that MNV replicate in viral factories having properties of liquid organelles[19,20,22–24] invites us to revisit the interplay between viral factories and the components of the cellular innate immunity. On one hand, the sequestration of viral RNAs in liquid compartments raises the question of their accessibility to cytosolic PRRs. On the other hand, the viral factories may sequester cellular proteins involved in innate immunity and keep them away from their functional signaling pathway. Here, we demonstrated that IFN production inhibitory forms of RABV P bind to phosphorylated TBK1 and interfere with TBK1 ability to assemble into liquid condensates formed in response to viral infection.

IFN induction is associated with the formation of liquid condensates

TBK1, NAP1, and SINTBAD form condensates in RABV-infected cells and more generally (at least for TBK1) upon exposure to danger signals such as extracellular and cytoplasmic dsRNA or lipofectamine depending on the cell line. In U-373MG cells infected with RABV, the formation of TBK1 condensates precedes IFN-β induction suggesting that they are required for this process.

TBK1 and SINTBAD condensates, which partially colocalize, have already been observed upon other cellular stresses.[55] Thus, condensate formation is a general feature in the signaling pathways involving those proteins.

TBK1 and NAP1 condensates are rather spherical which suggested that they were formed by LLPS. This was confirmed by the observation of fusion events between TBK1 condensates. Furthermore, a hypotonic shock causes the rapid dissolution of both TBK1 and NAP1 condensates followed by their reformation within a few minutes, which is a characteristic of several other liquid organelles including viral factories[19,51] and cellular Ddx4 organelles.[50]

The sensitivity of TBK1 and NAP1 condensates to their environment and the inability of antibodies to access the proteins inside such structures may explain why they have been rarely observed and described.[14,55] Indeed, classical PFA fixation protocols prevent the detection of TBK1 condensates. This suggests that beyond the field of innate immunity, signal transduction involves the formation of condensates that have not yet been observed.

Our data are consistent with an early formation of TBK1 condensates preceding TBK1 phosphorylation. Indeed, when TBK1^{KO} HAP1 cells overexpress either GFP-hTBK1-S172A or GFP-hTBK1-Y179A with mCherry-hNAP1, TBK1 condensates are observed. This indicates that TBK1 phosphorylation at S172 or Y179 site is not required for TBK1 condensate formation.

TBK1 condensates are dynamic. They can travel through the cytoplasm with rather straight trajectories. Their maximal speed is ~0.5–0.8 μm/s, consistent with those of other cargoes for which transport depends on microtubules.[56] On the other hand, TBK1 and NAP1 condensates can form larger aggregates having ring-like structures, in which they exhibit locally restricted movement. This particular pattern suggests that the aggregation occurs at the periphery of a bigger preexisting structure or compartment, so far unidentified, around which they move. The dynamics of those annular structures was assessed by FRAP which demonstrate that they exchange material with a cytoplasmic pool of TBK1 and NAP1 while retaining their shape.

Dynamic phase-separated condensates play a role all along the IFN-signaling pathway. Indeed, the cyclic GMP-AMP synthase (cGAS; a sensor of abnormal cytosolic dsDNA) forms liquid condensates with DNA,[57,58] the stimulator of IFN genes (STING) polymerizes upon activation[59] and makes condensates with stacked endoplasmic reticulum (ER) membrane,[60] and finally RIG-I and MDA-5 are resident proteins of antiviral SGs.[43,61–63] Here, we show that other liquid condensates are involved downstream in the signaling pathway underlining the importance of such processes in innate immunity.[64] It is tempting to speculate on the evolutionary reasons that led to the selection of such mechanisms. First, by concentrating proteins, the formation of such platforms, facilitates signal transduction and amplification as well as proximity-induced enzyme activation. Second, the dynamics of liquid condensates and their sensitivity to their physicochemical environment ensure a fast response (and its equally

rapid switching off) which can be further regulated by post-translational modifications. Third, LLPS is consistent with a threshold-like signaling response allowing a reaction to a danger signal that is an all-or-nothing process.[65] This is in agreement with observations showing that during an infection by an RNA virus, only a fraction of cells expresses IFN.[66,67] Alternatively, in the hypothesis that the cytosolic form of TBK1 would be the active form, the formation of condensates could buffer the concentration of free TBK1 in the cytosol and thus limit excessive responses.

The molecular bases of LLPS induced by TBK1 and its partner proteins remain to be investigated. It is worth noting that the latter contain predicted intrinsically disordered domains (IDDs) (Figure S7G), a feature which had been already noticed for SINTBAD[55] that contains particularly long IDDs, a characteristic often involved in LLPS.[68,69]

Finally, although TBK1 and NAP1 condensates colocalize, neither TBK1 nor NAP1 is required for the formation of condensates by the other protein in infected HAP1 cells. However, our experiments in which proteins were overexpressed (i.e., under conditions in which certain regulations can be circumvented) suggested that NAP1 is a positive regulator of TBK1 condensate formation, whereas TBK1 is a negative regulator of SINTBAD condensate formation.

RABV P binds to phosphorylated TBK1 and interferes with TBK1 condensate formation

Viruses have evolved mechanisms to delay or suppress both IFN production and signaling via the IFN-α/β receptor.[16] RABV P_{SAD} was known to inhibit the phosphorylation of IRF3, resulting in the inhibition of IFN production.[27] We show that it is not the case for RABV P_{CVS}. The phenotype of both strains can be switched by a single amino acid change in position 179 and the inhibitory phenotype is associated with P ability to bind phosphorylated TBK1. In IFN-producing U-373MG cells, SAD spreads more efficiently than SAD-S179P. In these cells, SAD infection induces a strong inhibition of IFN induction, associated with fewer TBK1 condensates compared with SAD-S179P infection. In N2A cells infected with SAD, TBK1 concentrates in NBs. This concentration of TBK1 in viral factories is not required for IFN inhibition as (1) in HEK293T transfected cells, P alone inhibits the IFN induction pathway, and (2) in U-373MG, TBK1 does not concentrate in NBs. Nevertheless, N2A cells in which TBK1 is associated with NBs contain fewer TBK1 condensates. Therefore, it is reasonable to speculate that TBK1 accumulation in NBs could enhance the inhibitory action of P.

The targeting of TBK1 is a particularly effective strategy to inhibit IFN production as TBK1 is located at the crossroads of several signaling pathways including those triggered by TLR3, RIG-I, and MDA-5 as well as STING.[45,70] Indeed, TBK1 is known to be targeted, directly or indirectly, by other viral proteins.[71] Among well-characterized examples are ICP27 from HSV1,[72] NS4B of HCV[73] and the sequestration of TBK1 into viral inclusion bodies by bunyaviruses.[74,75]

Interestingly, P may not be the only counteractant of the IFN-inducing pathway during RABV infection. The N protein of the Nishigahara RABV strain has also been shown to be involved in the pathway inhibition.[76] This underlines the importance for a virus to control the activation of the innate immune response.

Limitations of the study

Although our data are consistent with TBK1 condensate formation being required for IFN-β induction, we cannot rule out that this rather regulate the cytosolic concentration of TBK1. Furthermore, there might be several kinds of TBK1 condensates.[38,55,77] Here, in addition, we show that they can assemble into ring-like structures. Those distinct condensates, having distinct composition, may have distinct functions. Additional investigations will be required for a better understanding of their role as well as those of NAP1 and SINTBAD condensates.

Concluding remarks

The formation of innate immunity-associated condensates must be finely tuned to avoid inappropriate responses that may be harmful for the host. Indeed, we observed that NAP1, when overexpressed, already forms condensates and promotes TBK1 condensates assembly. On the other hand, TBK1 overexpression negatively regulates the formation of SINTBAD condensates. It is plausible that other proteins (including ISG products) affect the assembly of these condensates.

Thus, deregulation of condensate formation might explain certain phenotypes encountered in patients with mutations in genes involved in the signaling pathway.[78] Actually, mutations in genes encoding TBK1 or its partners that promote the formation of the condensates may be the cause of an overactivation of the IFN production pathway, leading to autoimmune diseases. Conversely, mutations that disadvantage the LLPS may result in an ineffective response to infections. This suggests that molecules stabilizing or destabilizing those innate immunity-associated liquid organelles may have therapeutic interest.

STAR★METHODS

Detailed methods are provided in the online version of this paper and include the following:

- KEY RESOURCES TABLE
- RESOURCE AVAILABILITY
  - Lead contact
  - Materials availability
  - Data and code availability
- EXPERIMENTAL MODEL AND SUBJECT DETAILS
  - Cell lines
  - Virus
  - Plasmids
- METHOD DETAILS
  - Antibodies and cell reagents
  - Viral infection
  - Construction and recovery of recombinant SAD virus expressing mutated phosphoprotein P
  - Titration of SAD and SAD-S179P viruses
  - Luciferase assay
  - Quantification of the expression of endogenous *IFN-β* gene
  - Western blot analysis
  - Immunoprecipitation for LC-MS/MS analysis
  - LC-MS/MS acquisition
  - LC-MS/MS data processing

- Co-immunoprecipitation of TBK1 with P protein
- Yeast two-hybrid (Y2H) system
- Yeast protein extraction
- Immunofluorescence staining and confocal microscopy
- Quantification of TBK1 condensates
- Live cell microscopy
- Image processing and analysis
- FRAP experiments

- QUANTIFICATION AND STATISTICAL ANALYSIS

SUPPLEMENTAL INFORMATION

Supplemental information can be found online at https://doi.org/10.1016/j.celrep.2022.111949.

ACKNOWLEDGMENTS

This work was supported by the Prix Bettencourt Coups d'Élan pour la Recherche Française attributed to Y.G., a grant from Agence Nationale de la Recherche, France (ANR CE11, LiquidFact) to Y.G. (including a post-doctoral grant to Q.N.), and a grant from Fondation pour la Recherche Médicale, France, to Y.G. (including a post-doctoral grant to D.G.). This work has benefited from the core facilities of Imagerie-Gif, supported by France-BioImaging (ANR-10-INBS-04-01). We thank Institut Jacques Monod, CNRS, Région Ile de France, and GIS IBiSA for financial support of the ProteoSeine@IJM platform. We thank Aurélie Albertini for careful reading of the manuscript.

AUTHOR CONTRIBUTIONS

Conceptualization, D.B., C.L.-G., and Y.G.; methodology, N.S., R.L.B., Q.N., D.G., D.B., C.L.-G., and Y.G.; investigations, N.S., Q.N., D.G., G.C., D.B., and C.L.-G; formal analysis, N.S., R.L.B., Q.N., D.G., G.C., A.C., D.B., C.L.-G., and Y.G.; supervision, D.B., C.L.-G., and Y.G.; funding acquisition, Y.G.; writing—original draft, C.L.-G. and Y.G.; writing—review and editing, N.S., R.L.B., Q.N., D.G., G.C., A.C., D.B., C.L.-G., and Y.G.

DECLARATION OF INTERESTS

The authors declare no competing interests.

INCLUSION AND DIVERSITY

We support inclusive, diverse, and equitable conduct of research.

Received: November 2, 2021
Revised: July 27, 2022
Accepted: December 19, 2022

REFERENCES

1. Mesev, E.V., LeDesma, R.A., and Ploss, A. (2019). Decoding type I and III interferon signalling during viral infection. Nat. Microbiol. *4*, 914–924. https://doi.org/10.1038/s41564-019-0421-x.
2. Teijaro, J.R. (2016). Type I interferons in viral control and immune regulation. Curr. Opin. Virol. *16*, 31–40. https://doi.org/10.1016/j.coviro.2016.01.001.
3. Schoggins, J.W. (2019). Interferon-stimulated genes: what do they all do? Annu. Rev. Virol. *6*, 567–584. https://doi.org/10.1146/annurev-virology-092818-015756.
4. de Oliveira Mann, C.C., and Hornung, V. (2021). Molecular mechanisms of nonself nucleic acid recognition by the innate immune system. Eur. J. Immunol. *51*, 1897–1910. https://doi.org/10.1002/eji.202049116.
5. Fitzgerald, K.A., and Kagan, J.C. (2020). Toll-like receptors and the control of immunity. Cell *180*, 1044–1066. https://doi.org/10.1016/j.cell.2020.02.041.
6. Alexopoulou, L., Holt, A.C., Medzhitov, R., and Flavell, R.A. (2001). Recognition of double-stranded RNA and activation of NF-kappaB by Toll-like receptor 3. Nature *413*, 732–738. https://doi.org/10.1038/35099560.
7. Diebold, S.S., Kaisho, T., Hemmi, H., Akira, S., and Reis e Sousa, C. (2004). Innate antiviral responses by means of TLR7-mediated recognition of single-stranded RNA. Science *303*, 1529–1531. https://doi.org/10.1126/science.1093616.
8. Fitzgerald, K.A., McWhirter, S.M., Faia, K.L., Rowe, D.C., Latz, E., Golenbock, D.T., Coyle, A.J., Liao, S.M., and Maniatis, T. (2003). IKKepsilon and TBK1 are essential components of the IRF3 signaling pathway. Nat. Immunol. *4*, 491–496. https://doi.org/10.1038/ni921.
9. Sharma, S., tenOever, B.R., Grandvaux, N., Zhou, G.P., Lin, R., and Hiscott, J. (2003). Triggering the interferon antiviral response through an IKK-related pathway. Science *300*, 1148–1151. https://doi.org/10.1126/science.1081315.
10. Yoo, J.S., Kato, H., and Fujita, T. (2014). Sensing viral invasion by RIG-I like receptors. Curr. Opin. Microbiol. *20*, 131–138. https://doi.org/10.1016/j.mib.2014.05.011.
11. Kowalinski, E., Lunardi, T., McCarthy, A.A., Louber, J., Brunel, J., Grigorov, B., Gerlier, D., and Cusack, S. (2011). Structural basis for the activation of innate immune pattern-recognition receptor RIG-I by viral RNA. Cell *147*, 423–435. https://doi.org/10.1016/j.cell.2011.09.039.
12. Wu, B., Peisley, A., Richards, C., Yao, H., Zeng, X., Lin, C., Chu, F., Walz, T., and Hur, S. (2013). Structural basis for dsRNA recognition, filament formation, and antiviral signal activation by MDA5. Cell *152*, 276–289. https://doi.org/10.1016/j.cell.2012.11.048.
13. Seth, R.B., Sun, L., Ea, C.K., and Chen, Z.J. (2005). Identification and characterization of MAVS, a mitochondrial antiviral signaling protein that activates NF-kappaB and IRF 3. Cell *122*, 669–682. https://doi.org/10.1016/j.cell.2005.08.012.
14. Goncalves, A., Bürckstümmer, T., Dixit, E., Scheicher, R., Górna, M.W., Karayel, E., Sugar, C., Stukalov, A., Berg, T., Kralovics, R., et al. (2011). Functional dissection of the TBK1 molecular network. PLoS One *6*, e23971. https://doi.org/10.1371/journal.pone.0023971.
15. Ryzhakov, G., and Randow, F. (2007). SINTBAD, a novel component of innate antiviral immunity, shares a TBK1-binding domain with NAP1 and TANK. EMBO J. *26*, 3180–3190. https://doi.org/10.1038/sj.emboj.7601743.
16. García-Sastre, A. (2017). Ten strategies of interferon Evasion by viruses. Cell Host Microbe *22*, 176–184. https://doi.org/10.1016/j.chom.2017.07.012.
17. Hampson, K., Coudeville, L., Lembo, T., Sambo, M., Kieffer, A., Attlan, M., Barrat, J., Blanton, J.D., Briggs, D.J., Cleaveland, S., et al. (2015). Estimating the global burden of endemic canine rabies. PLoS Negl. Trop. Dis. *9*, e0003709. https://doi.org/10.1371/journal.pntd.0003709.
18. Lahaye, X., Vidy, A., Pomier, C., Obiang, L., Harper, F., Gaudin, Y., and Blondel, D. (2009). Functional characterization of Negri bodies (NBs) in rabies virus-infected cells: Evidence that NBs are sites of viral transcription and replication. J. Virol. *83*, 7948–7958. https://doi.org/10.1128/JVI.00554-09.
19. Nikolic, J., Le Bars, R., Lama, Z., Scrima, N., Lagaudrière-Gesbert, C., Gaudin, Y., and Blondel, D. (2017). Negri bodies are viral factories with properties of liquid organelles. Nat. Commun. *8*, 58. https://doi.org/10.1038/s41467-017-00102-9.
20. Heinrich, B.S., Maliga, Z., Stein, D.A., Hyman, A.A., and Whelan, S.P.J. (2018). Phase transitions drive the Formation of vesicular stomatitis virus replication compartments. mBio *9*, 022900-17. https://doi.org/10.1128/mBio.02290-17.
21. Guseva, S., Milles, S., Jensen, M.R., Salvi, N., Kleman, J.P., Maurin, D., Ruigrok, R.W.H., and Blackledge, M. (2020). Measles virus nucleo- and phosphoproteins form liquid-like phase-separated compartments that promote nucleocapsid assembly. Sci. Adv. *6*, eaaz7095. https://doi.org/10.1126/sciadv.aaz7095.

22. Zhou, Y., Su, J.M., Samuel, C.E., and Ma, D. (2019). Measles virus forms inclusion bodies with properties of liquid organelles. J. Virol. *93*, 009488–e1019. https://doi.org/10.1128/JVI.00948-19.

23. Galloux, M., Risso-Ballester, J., Richard, C.A., Fix, J., Rameix-Welti, M.A., and Eleouet, J.F. (2020). Minimal elements required for the formation of respiratory syncytial virus cytoplasmic inclusion bodies in vivo and in vitro. mBio *11*. https://doi.org/10.1128/mBio.01202-20.

24. Rincheval, V., Lelek, M., Gault, E., Bouillier, C., Sitterlin, D., Blouquit-Laye, S., Galloux, M., Zimmer, C., Eleouet, J.F., and Rameix-Welti, M.A. (2017). Functional organization of cytoplasmic inclusion bodies in cells infected by respiratory syncytial virus. Nat. Commun. *8*, 563. https://doi.org/10.1038/s41467-017-00655-9.

25. Chelbi-Alix, M.K., Vidy, A., El Bougrini, J., and Blondel, D. (2006). Rabies viral mechanisms to escape the IFN system: the viral protein P interferes with IRF-3, Stat1, and PML nuclear bodies. J. Interferon Cytokine Res. *26*, 271–280. https://doi.org/10.1089/jir.2006.26.271.

26. Ito, N., Moseley, G.W., Blondel, D., Shimizu, K., Rowe, C.L., Ito, Y., Masatani, T., Nakagawa, K., Jans, D.A., and Sugiyama, M. (2010). Role of interferon antagonist activity of rabies virus phosphoprotein in viral pathogenicity. J. Virol. *84*, 6699–6710. https://doi.org/10.1128/JVI.00011-10.

27. Brzózka, K., Finke, S., and Conzelmann, K.K. (2005). Identification of the rabies virus alpha/beta interferon antagonist: phosphoprotein P interferes with phosphorylation of interferon regulatory factor 3. J. Virol. *79*, 7673–7681. https://doi.org/10.1128/JVI.79.12.7673-7681.2005.

28. Vidy, A., Chelbi-Alix, M., and Blondel, D. (2005). Rabies virus P protein interacts with STAT1 and inhibits interferon signal transduction pathways. J. Virol. *79*, 14411–14420. https://doi.org/10.1128/JVI.79.22.14411-14420.2005.

29. Brzózka, K., Finke, S., and Conzelmann, K.K. (2006). Inhibition of interferon signaling by rabies virus phosphoprotein P: activation-dependent binding of STAT1 and STAT2. J. Virol. *80*, 2675–2683. https://doi.org/10.1128/JVI.80.6.2675-2683.2006.

30. Vidy, A., El Bougrini, J., Chelbi-Alix, M.K., and Blondel, D. (2007). The nucleocytoplasmic rabies virus P protein counteracts interferon signaling by inhibiting both nuclear accumulation and DNA binding of STAT1. J. Virol. *81*, 4255–4263. https://doi.org/10.1128/JVI.01930-06.

31. Blondel, D., Regad, T., Poisson, N., Pavie, B., Harper, F., Pandolfi, P.P., De Thé, H., and Chelbi-Alix, M.K. (2002). Rabies virus P and small P products interact directly with PML and reorganize PML nuclear bodies. Oncogene *21*, 7957–7970. https://doi.org/10.1038/sj.onc.1205931.

32. Blondel, D., Kheddache, S., Lahaye, X., Dianoux, L., and Chelbi-Alix, M.K. (2010). Resistance to rabies virus infection conferred by the PMLIV isoform. J. Virol. *84*, 10719–10726. https://doi.org/10.1128/JVI.01286-10.

33. Yoneyama, M., Kikuchi, M., Natsukawa, T., Shinobu, N., Imaizumi, T., Miyagishi, M., Taira, K., Akira, S., and Fujita, T. (2004). The RNA helicase RIG-I has an essential function in double-stranded RNA-induced innate antiviral responses. Nat. Immunol. *5*, 730–737. https://doi.org/10.1038/ni1087.

34. Rieder, M., Brzózka, K., Pfaller, C.K., Cox, J.H., Stitz, L., and Conzelmann, K.K. (2011). Genetic dissection of interferon-antagonistic functions of rabies virus phosphoprotein: inhibition of interferon regulatory factor 3 activation is important for pathogenicity. J. Virol. *85*, 842–852. https://doi.org/10.1128/JVI.01427-10.

35. Chang, T.H., Liao, C.L., and Lin, Y.L. (2006). Flavivirus induces interferon-beta gene expression through a pathway involving RIG-I-dependent IRF-3 and PI3K-dependent NF-kappaB activation. Microbes Infect. *8*, 157–171. https://doi.org/10.1016/j.micinf.2005.06.014.

36. Lahaye, X., Vidy, A., Fouquet, B., and Blondel, D. (2012). Hsp70 protein positively regulates rabies virus infection. J. Virol. *86*, 4743–4751. https://doi.org/10.1128/JVI.06501-11.

37. Raux, H., Flamand, A., and Blondel, D. (2000). Interaction of the rabies virus P protein with the LC8 dynein light chain. J. Virol. *74*, 10212–10216. https://doi.org/10.1128/jvi.74.21.10212-10216.2000.

38. Pillai, S., Nguyen, J., Johnson, J., Haura, E., Coppola, D., and Chellappan, S. (2015). Tank binding kinase 1 is a centrosome-associated kinase necessary for microtubule dynamics and mitosis. Nat. Commun. *6*, 10072. https://doi.org/10.1038/ncomms10072.

39. Larabi, A., Devos, J.M., Ng, S.L., Nanao, M.H., Round, A., Maniatis, T., and Panne, D. (2013). Crystal structure and mechanism of activation of TANK-binding kinase 1. Cell Rep. *3*, 734–746. https://doi.org/10.1016/j.celrep.2013.01.034.

40. Ma, X., Helgason, E., Phung, Q.T., Quan, C.L., Iyer, R.S., Lee, M.W., Bowman, K.K., Starovasnik, M.A., and Dueber, E.C. (2012). Molecular basis of Tank-binding kinase 1 activation by transautophosphorylation. Proc. Natl. Acad. Sci. USA. *109*, 9378–9383. https://doi.org/10.1073/pnas.1121552109.

41. Tu, D., Zhu, Z., Zhou, A.Y., Yun, C.H., Lee, K.E., Toms, A.V., Li, Y., Dunn, G.P., Chan, E., Thai, T., et al. (2013). Structure and ubiquitination-dependent activation of TANK-binding kinase 1. Cell Rep. *3*, 747–758. https://doi.org/10.1016/j.celrep.2013.01.033.

42. Li, X., Yang, M., Yu, Z., Tang, S., Wang, L., Cao, X., and Chen, T. (2017). The tyrosine kinase Src promotes phosphorylation of the kinase TBK1 to facilitate type I interferon production after viral infection. Sci. Signal. *10*, eaae0435. https://doi.org/10.1126/scisignal.aae0435.

43. Nikolic, J., Civas, A., Lama, Z., Lagaudrière-Gesbert, C., and Blondel, D. (2016). Rabies virus infection induces the Formation of stress granules closely connected to the viral factories. PLoS Pathog. *12*, e1005942. https://doi.org/10.1371/journal.ppat.1005942.

44. Yang, P., Mathieu, C., Kolaitis, R.M., Zhang, P., Messing, J., Yurtsever, U., Yang, Z., Wu, J., Li, Y., Pan, Q., et al. (2020). G3BP1 is a tunable switch that triggers phase separation to assemble stress granules. Cell *181*, 325–345.e28. https://doi.org/10.1016/j.cell.2020.03.046.

45. Helgason, E., Phung, Q.T., and Dueber, E.C. (2013). Recent insights into the complexity of Tank-binding kinase 1 signaling networks: the emerging role of cellular localization in the activation and substrate specificity of TBK1. FEBS Lett. *587*, 1230–1237. https://doi.org/10.1016/j.febslet.2013.01.059.

46. Li, S., Wang, L., Berman, M., Kong, Y.Y., and Dorf, M.E. (2011). Mapping a dynamic innate immunity protein interaction network regulating type I interferon production. Immunity *35*, 426–440. https://doi.org/10.1016/j.immuni.2011.06.014.

47. Sato, S., Sugiyama, M., Yamamoto, M., Watanabe, Y., Kawai, T., Takeda, K., and Akira, S. (2003). Toll/IL-1 receptor domain-containing adaptor inducing IFN-beta (TRIF) associates with TNF receptor-associated factor 6 and TANK-binding kinase 1, and activates two distinct transcription factors, NF-kappa B and IFN-regulatory factor-3, in the Toll-like receptor signaling. J. Immunol. *171*, 4304–4310. https://doi.org/10.4049/jimmunol.171.8.4304.

48. Mankouri, J., Fragkoudis, R., Richards, K.H., Wetherill, L.F., Harris, M., Kohl, A., Elliott, R.M., and Macdonald, A. (2010). Optineurin negatively regulates the induction of IFNbeta in response to RNA virus infection. PLoS Pathog. *6*, e1000778. https://doi.org/10.1371/journal.ppat.1000778.

49. Outlioua, A., Pourcelot, M., and Arnoult, D. (2018). The role of optineurin in antiviral type I interferon production. Front. Immunol. *9*, 853. https://doi.org/10.3389/fimmu.2018.00853.

50. Nott, T.J., Petsalaki, E., Farber, P., Jervis, D., Fussner, E., Plochowietz, A., Craggs, T.D., Bazett-Jones, D.P., Pawson, T., Forman-Kay, J.D., and Baldwin, A.J. (2015). Phase transition of a disordered nuage protein generates environmentally responsive membraneless organelles. Mol. Cell *57*, 936–947. https://doi.org/10.1016/j.molcel.2015.01.013.

51. Risso-Ballester, J., Galloux, M., Cao, J., Le Goffic, R., Hontonnou, F., Jobart-Malfait, A., Desquesnes, A., Sake, S.M., Haid, S., Du, M., et al. (2021). A condensate-hardening drug blocks RSV replication in vivo. Nature *595*, 596–599. https://doi.org/10.1038/s41586-021-03703-z.

52. Gapp, B.V., Konopka, T., Penz, T., Dalal, V., Bürckstümmer, T., Bock, C., and Nijman, S.M. (2016). Parallel reverse genetic screening in mutant human cells using transcriptomics. Mol. Syst. Biol. *12*, 879. https://doi.org/10.15252/msb.20166890.

53. Guo, X., Wang, H., Li, Y., Leng, X., Huang, W., Ma, Y., Xu, T., and Qi, X. (2019). Transfection reagent Lipofectamine triggers type I interferon signaling activation in macrophages. Immunol. Cell Biol. *97*, 92–96. https://doi.org/10.1111/imcb.12194.

54. Li, X.L., Boyanapalli, M., Weihua, X., Kalvakolanu, D.V., and Hassel, B.A. (1998). Induction of interferon synthesis and activation of interferon-stimulated genes by liposomal transfection reagents. J. Interferon Cytokine Res. *18*, 947–952. https://doi.org/10.1089/jir.1998.18.947.

55. Saul, V.V., Seibert, M., Krüger, M., Jeratsch, S., Kracht, M., and Schmitz, M.L. (2019). ULK1/2 restricts the formation of inducible SINT-speckles, membraneless organelles controlling the threshold of TBK1 activation. iScience *19*, 527–544. https://doi.org/10.1016/j.isci.2019.08.001.

56. Hunter, B., and Allingham, J.S. (2020). These motors were made for walking. Protein Sci. *29*, 1707–1723. https://doi.org/10.1002/pro.3895.

57. Du, M., and Chen, Z.J. (2018). DNA-induced liquid phase condensation of cGAS activates innate immune signaling. Science *361*, 704–709. https://doi.org/10.1126/science.aat1022.

58. Xie, W., Lama, L., Adura, C., Tomita, D., Glickman, J.F., Tuschl, T., and Patel, D.J. (2019). Human cGAS catalytic domain has an additional DNA-binding interface that enhances enzymatic activity and liquid-phase condensation. Proc. Natl. Acad. Sci. USA. *116*, 11946–11955. https://doi.org/10.1073/pnas.1905013116.

59. Ergun, S.L., Fernandez, D., Weiss, T.M., and Li, L. (2019). STING polymer structure reveals mechanisms for activation, hyperactivation, and inhibition. Cell *178*, 290–301.e10. https://doi.org/10.1016/j.cell.2019.05.036.

60. Yu, X., Zhang, L., Shen, J., Zhai, Y., Jiang, Q., Yi, M., Deng, X., Ruan, Z., Fang, R., Chen, Z., et al. (2021). The STING phase-separator suppresses innate immune signalling. Nat. Cell Biol. *23*, 330–340. https://doi.org/10.1038/s41556-021-00659-0.

61. Kim, S.S.Y., Sze, L., Liu, C., and Lam, K.P. (2019). The stress granule protein G3BP1 binds viral dsRNA and RIG-I to enhance interferon-beta response. J. Biol. Chem. *294*, 6430–6438. https://doi.org/10.1074/jbc.RA118.005868.

62. Onomoto, K., Jogi, M., Yoo, J.S., Narita, R., Morimoto, S., Takemura, A., Sambhara, S., Kawaguchi, A., Osari, S., Nagata, K., et al. (2012). Critical role of an antiviral stress granule containing RIG-I and PKR in viral detection and innate immunity. PLoS One *7*, e43031. https://doi.org/10.1371/journal.pone.0043031.

63. Yang, W., Ru, Y., Ren, J., Bai, J., Wei, J., Fu, S., Liu, X., Li, D., and Zheng, H. (2019). G3BP1 inhibits RNA virus replication by positively regulating RIG-I-mediated cellular antiviral response. Cell Death Dis. *10*, 946. https://doi.org/10.1038/s41419-019-2178-9.

64. Xiao, Q., McAtee, C.K., and Su, X. (2021). Phase separation in immune signalling. Nat. Rev. Immunol. *22*, 188–199. https://doi.org/10.1038/s41577-021-00572-5.

65. Shi, M., Zhang, P., Vora, S.M., and Wu, H. (2020). Higher-order assemblies in innate immune and inflammatory signaling: a general principle in cell biology. Curr. Opin. Cell Biol. *63*, 194–203. https://doi.org/10.1016/j.ceb.2020.03.002.

66. Killip, M.J., Jackson, D., Pérez-Cidoncha, M., Fodor, E., and Randall, R.E. (2017). Single-cell studies of IFN-beta promoter activation by wild-type and NS1-defective influenza A viruses. J. Gen. Virol. *98*, 357–363. https://doi.org/10.1099/jgv.0.000687.

67. Killip, M.J., Young, D.F., Ross, C.S., Chen, S., Goodbourn, S., and Randall, R.E. (2011). Failure to activate the IFN-beta promoter by a paramyxovirus lacking an interferon antagonist. Virology *415*, 39–46. https://doi.org/10.1016/j.virol.2011.03.027.

68. Alberti, S., Gladfelter, A., and Mittag, T. (2019). Considerations and challenges in studying liquid-liquid phase separation and biomolecular condensates. Cell *176*, 419–434. https://doi.org/10.1016/j.cell.2018.12.035.

69. Uversky, V.N. (2017). Intrinsically disordered proteins in overcrowded milieu: membrane-less organelles, phase separation, and intrinsic disorder. Curr. Opin. Struct. Biol. *44*, 18–30. https://doi.org/10.1016/j.sbi.2016.10.015.

70. Zhou, R., Zhang, Q., and Xu, P. (2020). TBK1, a central kinase in innate immune sensing of nucleic acids and beyond. Acta Biochim. Biophys. Sin. *52*, 757–767. https://doi.org/10.1093/abbs/gmaa051.

71. Zhao, W. (2013). Negative regulation of TBK1-mediated antiviral immunity. FEBS Lett. *587*, 542–548. https://doi.org/10.1016/j.febslet.2013.01.052.

72. Christensen, M.H., Jensen, S.B., Miettinen, J.J., Luecke, S., Prabakaran, T., Reinert, L.S., Mettenleiter, T., Chen, Z.J., Knipe, D.M., Sandri-Goldin, R.M., et al. (2016). HSV-1 ICP27 targets the TBK1-activated STING signalsome to inhibit virus-induced type I IFN expression. EMBO J. *35*, 1385–1399. https://doi.org/10.15252/embj.201593458.

73. Ding, Q., Cao, X., Lu, J., Huang, B., Liu, Y.J., Kato, N., Shu, H.B., and Zhong, J. (2013). Hepatitis C virus NS4B blocks the interaction of STING and TBK1 to evade host innate immunity. J. Hepatol. *59*, 52–58. https://doi.org/10.1016/j.jhep.2013.03.019.

74. Santiago, F.W., Covaleda, L.M., Sanchez-Aparicio, M.T., Silvas, J.A., Diaz-Vizarreta, A.C., Patel, J.R., Popov, V., Yu, X.J., García-Sastre, A., and Aguilar, P.V. (2014). Hijacking of RIG-I signaling proteins into virus-induced cytoplasmic structures correlates with the inhibition of type I interferon responses. J. Virol. *88*, 4572–4585. https://doi.org/10.1128/JVI.03021-13.

75. Wu, X., Qi, X., Qu, B., Zhang, Z., Liang, M., Li, C., Cardona, C.J., Li, D., and Xing, Z. (2014). Evasion of antiviral immunity through sequestering of TBK1/IKKepsilon/IRF3 into viral inclusion bodies. J. Virol. *88*, 3067–3076. https://doi.org/10.1128/JVI.03510-13.

76. Masatani, T., Ito, N., Shimizu, K., Ito, Y., Nakagawa, K., Sawaki, Y., Koyama, H., and Sugiyama, M. (2010). Rabies virus nucleoprotein functions to evade activation of the RIG-I-mediated antiviral response. J. Virol. *84*, 4002–4012. https://doi.org/10.1128/JVI.02220-09.

77. Rudashevskaya, E.L., Sacco, R., Kratochwill, K., Huber, M.L., Gstaiger, M., Superti-Furga, G., and Bennett, K.L. (2013). A method to resolve the composition of heterogeneous affinity-purified protein complexes assembled around a common protein by chemical cross-linking, gel electrophoresis and mass spectrometry. Nat. Protoc. *8*, 75–97. https://doi.org/10.1038/nprot.2012.133.

78. Zhang, Q., Bastard, P., Liu, Z., Le Pen, J., Moncada-Velez, M., Chen, J., Ogishi, M., Sabli, I.K.D., Hodeib, S., Korol, C., et al. (2020). Inborn errors of type I IFN immunity in patients with life-threatening COVID-19. Science *370*, eabd4570. https://doi.org/10.1126/science.abd4570.

79. Raux, H., Iseni, F., Lafay, F., and Blondel, D. (1997). Mapping of monoclonal antibody epitopes of the rabies virus P protein. J. Gen. Virol. *78*, 119–124. https://doi.org/10.1099/0022-1317-78-1-119.

80. Schnell, M.J., Mebatsion, T., and Conzelmann, K.K. (1994). Infectious rabies viruses from cloned cDNA. EMBO J. *13*, 4195–4203.

81. Seif, I., Coulon, P., Rollin, P.E., and Flamand, A. (1985). Rabies virulence: effect on pathogenicity and sequence characterization of rabies virus mutations affecting antigenic site III of the glycoprotein. J. Virol. *53*, 926–934. https://doi.org/10.1128/JVI.53.3.926-934.1985.

82. Perez-Riverol, Y., Csordas, A., Bai, J., Bernal-Llinares, M., Hewapathirana, S., Kundu, D.J., Inuganti, A., Griss, J., Mayer, G., Eisenacher, M., et al. (2019). The PRIDE database and related tools and resources in 2019: improving support for quantification data. Nucleic Acids Res. *47*, D442–D450. https://doi.org/10.1093/nar/gky1106.

83. Buchholz, U.J., Finke, S., and Conzelmann, K.K. (1999). Generation of bovine respiratory syncytial virus (BRSV) from cDNA: BRSV NS2 is not essential for virus replication in tissue culture, and the human RSV leader region acts as a functional BRSV genome promoter. J. Virol. *73*, 251–259. https://doi.org/10.1128/JVI.73.1.251-259.1999.

84. Schneider, C.A., Rasband, W.S., and Eliceiri, K.W. (2012). NIH Image to ImageJ: 25 years of image analysis. Nat. Methods *9*, 671–675. https://doi.org/10.1038/nmeth.2089.

85. Schindelin, J., Arganda-Carreras, I., Frise, E., Kaynig, V., Longair, M., Pietzsch, T., Preibisch, S., Rueden, C., Saalfeld, S., Schmid, B., et al. (2012). Fiji: an open-source platform for biological-image analysis. Nat. Methods *9*, 676–682. https://doi.org/10.1038/nmeth.2019.

86. Fouquet, B., Nikolic, J., Larrous, F., Bourhy, H., Wirblich, C., Lagaudrière-Gesbert, C., and Blondel, D. (2015). Focal adhesion kinase is involved in rabies virus infection through its interaction with viral phosphoprotein P. J. Virol. *89*, 1640–1651. https://doi.org/10.1128/JVI.02602-14.

87. Finke, S., and Conzelmann, K.K. (1999). Virus promoters determine interference by defective RNAs: selective amplification of mini-RNA vectors and rescue from cDNA by a 3' copy-back ambisense rabies virus. J. Virol. *73*, 3818–3825. https://doi.org/10.1128/JVI.73.5.3818-3825.1999.

88. Génin, P., Lin, R., Hiscott, J., and Civas, A. (2009). Differential regulation of human interferon A gene expression by interferon regulatory factors 3 and 7. Mol. Cell Biol. *29*, 3435–3450. https://doi.org/10.1128/MCB.01805-08.

89. Diel, E.E., Lichtman, J.W., and Richardson, D.S. (2020). Tutorial: avoiding and correcting sample-induced spherical aberration artifacts in 3D fluorescence microscopy. Nat. Protoc. *15*, 2773–2784. https://doi.org/10.1038/s41596-020-0360-2.

90. Tinevez, J.Y., Perry, N., Schindelin, J., Hoopes, G.M., Reynolds, G.D., Laplantine, E., Bednarek, S.Y., Shorte, S.L., and Eliceiri, K.W. (2017). TrackMate: an open and extensible platform for single-particle tracking. Methods *115*, 80–90. https://doi.org/10.1016/j.ymeth.2016.09.016.

STAR★METHODS

KEY RESOURCES TABLE

REAGENT or RESOURCE	SOURCE	IDENTIFIER
Antibodies		
Rabbit polyclonal anti-P (5.2)	Lahaye et al.[18]	N/A
Rabbit monoclonal anti-P (26G6)	Raux et al.[79]	N/A
Rabbit monoclonal anti-P (31G10)	Raux et al.[79]	N/A
Mouse monoclonal anti-N (81C4)	Nikolic et al.[19]	N/A
Mouse monoclonal anti-α-Tubulin	Sigma-Aldrich	Cat# T6199; RRID:AB_477583
Rabbit monoclonal anti-NAK/TBK1 (clone EP611Y)	Abcam	Cat# ab40676; RRID:AB_776632
Rabbit monoclonal anti-phospho-TBK1/NAK (Ser172) (clone D52C2)	Cell signaling Technology	Cat#5483; RRID:AB_10693472
Rabbit polyclonal anti-IRF3 (FL-425)	Santa Cruz Biotechnology	Cat# sc-9082; RRID:AB_2264929
Mouse monoclonal anti-GFP (7.1 and 13.1)	Roche Diagnostics	Cat# 11 814,460 001; RRID:AB_390913
Mouse monoclonal anti-G3BP (clone 2F3)	Sigma-Aldrich	Cat#WH0010146M1; RRID:AB_1841708
Mouse monoclonal DYKDDDDK Tag (clone 9A3)	Cell signaling Technology	Cat#8146; RRID:AB_10950495
Rabbit monoclonal anti-AZI2 (clone EPR14698)	Abcam	Cat#ab192253
Rabbit polyclonal anti-TBKBP1 (SINTBAD)	Abcam	Cat#ab106394; RRID:AB_10863878
Rabbit polyclonal anti-TANK/TRAF2	Abcam	Cat#ab47632; RRID:AB_882837
Rabbit polyclonal anti-OPTN	Thermo Fisher Scientific	Cat #PA5-51882; RRID:AB_2644993
Rabbit polyclonal anti-TRIF	Thermo Fisher Scientific	Cat# PA5-88150; RRID:AB_2804692
Rabbit monoclonal anti- DYNLL1 (LC8) (EPI660Y)	Abcam	Cat#ab51603; RRID:AB_2093654
Rabbit polyclonal anti- Stat1 p84/p91 (clone E−23)	Santa Cruz Biotechnology	Cat#Sc-346; RRID:AB_632435
Rabbit polyclonal anti-MAVS/VISA	Bethyl laboratories	Cat#A300-782A; RRID:AB_669744
Alexa 488 goat anti-rabbit IgG	Thermo Fisher Scientific	Cat#A-11008
Alexa 488 goat anti-mouse IgG	Thermo Fisher Scientific	Cat# A-11029
Alexa 568 goat anti-mouse IgG	Thermo Fisher Scientific	Cat# A-11031
Alexa 568 goat anti-rabbit IgG	Thermo Fisher Scientific	Cat# A-11011
Alexa 647 goat anti-rabbit IgG	Thermo Fisher Scientific	Cat# A-21246
Anti-rabbit 800-conjugated IgG	Cell signaling Technology	Cat#5151
Anti-mouse 680-conjugated IgG	Cell signaling Technology	Cat#5470
Goat anti-rabbit IgG, HRP	Invitrogen	Cat#31460
Goat anti-mouse IgG, HRP	Sigma-Aldrich	Cat# A4416
Bacterial and virus strains		
RABV SAD L16-B19	Schnell et al.[80]	N/A
RABV Challenge Virus Standard (CVS)	Seif et al.[81]	N/A
Chemicals, peptides, and recombinant proteins		
MitoTracker Red CMXRos	Cell Signaling Technology	Cat#9082
FM4-64FX	Molecular Probes	Cat#F34653
5′ triphosphate double-stranded RNA	InvivoGen	Cat#tlrl-3prna
Dual-Luciferase Reporter Assay System	Promega	Cat# E1910
DSP (dithiobis[succinimidylpropionate])	Thermo Fisher Scientific	Cat# 22585
High Capacity cDNA Reverse Transcription Kit	Applied Biosystems	Cat# 4368814
SYBR green PCR master mix	Applied Biosystems	Cat# 4309155

(*Continued on next page*)

CellPress
OPEN ACCESS

Continued

REAGENT or RESOURCE	SOURCE	IDENTIFIER
Anti-FLAG M2 Magnetic Beads	Sigma-Aldrich	Cat#M8823
Protein A Magnetic Beads	Pierce	Cat# 88845
Deposited data		
The mass spectrometry proteomics data have been deposited to the ProteomeXchange consortium via the PRIDE partner repository	Perez-Riverol et al.[82]	ProteomeXchange: PXD028740
Experimental models: Cell lines		
Human embryonic kidney 293T cells (HEK293T)	ATCC	Cat#CRL-3216; RRID:CVCL_0063
Mouse: Neuro-2a cells (N2A)	ATCC	Cat#CCL-131; RRID:CVCL_0470
Human glioblastoma astrocytoma cells (U-373MG)	ATCC	Cat# HTB-17; RRID:CVCL_2219
Hamster: baby hamster kidney cells (BSR), clone form BHK-21	Dr A. Flamand (Former Laboratoire de Génétique des Virus, Gif-sur-Yvette, France)	N/A
Hamster: BSR-T7/5	Buchholz et al.[83]	RRID:CVCL_RW96
Human HAP1 parental control cell line	Horizon discovery	Cat#C631; RRID:CVCL_Y019
Human TBK1 knockout cell line	Horizon Discovery	Cat#HZGHC000031c010; RRID:CVCL_TR72
Human AZI2 knockout cell line	Horizon Discovery	Cat#HZGHC003895c005; RRID:CVCL_SE40
Human MAVS knockout cell line	Horizon Discovery	Cat#HZGHC001456c011; RRID:CVCL_SX36
Experimental models: Organisms/strains		
Saccharomyces cerevisiae Hansen cells (L40)	ATCC	Cat#MYA-3332
Oligonucleotides		
GAPDH_Human_For: AACAGCCTCAAGATCATCAGCAA	qPCR; This paper	N/A
GAPDH_Human_Rev: TCTTCTGGGTGGCAGTGAT	qPCR; This paper	N/A
GAPDH_Mouse_For: TCAACTACATGGTCTACATGTT	qPCR; This paper	N/A
GAPDH_Mouse_Rev: GGTCTCGCTCCTGGAAGA	qPCR; This paper	N/A
IFN-β_Human_For: GTCTCCTCCAAATTGCTCTC	qPCR; This paper	N/A
IFN-β_Human_Rev: ACAGGAGCTTCTCACACTGA	qPCR; This paper	N/A
IFN-β_Mouse_For: GGAGATGACGGAGAAGATGC	qPCR; This paper	N/A
IFN-β_Mouse_Rev: CCCAGTGCTGGAGAAATTGT	qPCR; This paper	N/A
Recombinant DNA		
See Table S1		N/A
Software and algorithms		
Image Studio	LI-COR, Lincoln, NE	Version 5.2
PEAKS Online Xpro	Bioinformatics Solutions Inc.	N/A
Qlucore Omics Explorer	Qlucore AB	Version 3.7
ImageJ	Schneider et al.[84]	https://imagej.nih.gov/ij/
FIJI	Schindelin et al.[85]	N/A

(*Continued on next page*)

Continued

REAGENT or RESOURCE	SOURCE	IDENTIFIER
Huygens Essential 22.04	Scientific Volume Imaging B.V.	N/A
MetaMorph	Molecular Devices	Version 7.7
Prism	GraphPad	Version 9.4.1
Leica Application Suite X (LAS X)	Leica	N/A
Zen 2.3 pro	Zeiss	N/A
Imaris	Oxford instruments	Version 9.3

RESOURCE AVAILABILITY

Lead contact

Further information and requests for resources and reagents should be directed to and will be fulfilled by the lead contact, Yves Gaudin (yves.gaudin@i2bc.paris-saclay.fr).

Materials availability

All unique and stable reagents generated in this study are available from the lead contact with a completed Materials Transfer Agreement.

Data and code availability

Mass spectrometry data have been deposited in the ProteomeXchange Consortium via the PRIDE partner repository. Accession number is indicated in the key resources table.

This paper does not report original code.

Any additional information required to reanalyze the data reported in this paper is available from the lead contact upon request.

EXPERIMENTAL MODEL AND SUBJECT DETAILS

Cell lines

HEK293T cells (human embryonic kidney, ATCC #CRL-3216), N2A cells (mouse neuroblastoma, ATCC #CCL-131) and U-373MG cells (human glioblastoma astrocytoma) were purchased from ATCC organization (http://www.lgcstandards-atcc.org). BSR cells, a clone from BHK 21 (Baby Hamster Kidney) were obtained from Dr A. Flamand (Former Laboratoire de Génétique des Virus, Gif-sur-Yvette, France). BSR-T7/5 cell line is a clone of BHK 21 constitutively expressing the T7 RNA polymerase.[83] All these cells were grown in Dulbecco's modified eagle medium (DMEM) (Gibco-Life Technologies) supplemented with 10% fetal calf serum (FCS) (Gibco-Life Technologies) and 100 units/mL of Penicillin and 100 μg/mL of Streptomycin (AB 1X) (Gibco-Life Technologies). BSR-T7/5 cells were grown in the same medium supplemented with 1 mg/mL Geneticin (Gibco-Life Technologies).

Human HAP1 parental control cells (#C631), TBK1^{KO} HAP1 cells (#HZGHC000031c010), NAP1^{KO} HAP1 (#HZGHC003895c005), and MAVS^{KO} HAP1 cells (#HZGHC001456c011) were purchased form Horizon Discovery (https://horizondiscovery.com/en/engineered-cell-lines). All these cells were grown in Iscove's Modification from DMEM (IMDM, Corning) supplemented with 10% FCS and 100 units/mL of penicillin and 100 μg/mL of Streptomycin (AB 1X).

Virus

Recombinant RABV SAD L16-B19 (called SAD all along the text),[80] recombinant SAD-S179P (see below), and the Challenge Virus Standard (CVS)[81] were grown on BSR cells.

Plasmids

For all plasmid constructs, please refer to the recombinant DNA Table S1. Briefly, the plasmid pcDNA3.1 hygro(−) encoding P protein of CVS strain, referred to as pP_{CVS}, has been previously described[86] whereas the one encoding P protein of SAD strain, referred to as pP_{SAD}, was constructed on purpose for this work. The plasmids pTit encoding P protein of SAD and CVS strains, referred to as pTit-P_{SAD} and pTit-P_{CVS}, have been previously described.[19,87] In pTit plasmids,[83,87] the gene of interest is under the dependence of the T7 polymerase promoter and the corresponding transcripts contain an internal ribosomal entry site (IRES) located upstream the open reading frame.

Point mutation mutants either in *P* or in *TBK1* genes were constructed by using QuikChange Site-Directed Mutagenesis Kit (Agilent Technologies).

For pP_{SAD}-FLAG, pP_{SAD}-S179P-FLAG, pP_{CVS}-FLAG and pP_{CVS}-P179S-FLAG, the fragments were amplified by PCR using Phusion Polymerase (New England Biolabs) and inserted into the NheI/XhoI restriction sites of pcDNA3.1 hygro(−).

The synthetic genes encoding mouse TBK1 protein, mouse and human NAP1 proteins, and mouse SINTBAD protein were obtained from Twist Bioscience and inserted into the NheI/NotI restriction sites of pcDNA3.1 hygro(−). Plasmids encoding mouse and human TBK1 or the adaptor proteins amino-terminally fused to the GFP or to the mCherry as well as those encoding FLAG-TBK1 were constructed using Gibson assembly kit (New England Biolabs).

Plasmid pEF6FLAGΔRIG-I was previously described.[33] The sequence coding ΔRIG-I (i.e. without FLAG) was subcloned into empty vector pEF6/myc-His B (Invitrogen). Plasmid pIRF3-5D as well as the plasmid from which human hTBK1 gene was subcloned have been previously described.[35,88]

The yeast expression plasmids pLexA and pGAD were previously described.[37] The vector pLexA contains the yeast selectable gene TRP1 and the LexA DNA-binding domain (BD) (202 residues) coding sequence. The plasmid pGAD contains the yeast selectable gene LEU2 and the sequence encoding the GAL4 activation domain (AD) (amino acids 768 to 884). These plasmids were used for the expression of fusion proteins.

METHOD DETAILS

Antibodies and cell reagents

The rabbit polyclonal anti-P antibody was previously described[18] and was used at a 1:2000 dilution for immunofluorescence (IF) staining and 1:1000 for western blot (WB) analysis. Anti-P mouse monoclonal antibody 26G6 was previously described and used for WB analysis.[79] Anti P mouse monoclonal antibody 31G10, although not described in the article, comes from the same collection as antibody 26G6 and was used for P immunoprecipitation. Mouse monoclonal anti-N antibody (81C4), was previously described[19] and was used for IF staining. The mouse monoclonal anti-α-Tubulin (#T6199, Sigma Aldrich) antibody was used at a 1:1000 dilution. The rabbit monoclonal anti-NAK/TBK1 antibody (EP611Y, Abcam) was used at a 1:250 dilution for IF staining and 1:1000 for WB analysis. The rabbit monoclonal anti-Phospho-TBK1/NAK (Ser172) (D52C2, Cell Signaling) antibody, directed against TBK1 phosphorylated form on serine 172 and referred to as anti-pTBK1(S172) in the text, was used at a 1:50 dilution for IF staining and 1:1000 for WB analysis. The rabbit polyclonal anti-IRF3 (FL-425, Santa Cruz Biotechnology) was used at 1:100 dilution. Mouse monoclonal anti-GFP antibodies (7.1 and 13.1, Roche Diagnostics) were used at a 1:1000 dilution for WB analysis. The mouse monoclonal anti-G3BP1 (2F3, Sigma Aldrich) antibody was used at a 1:50 dilution. The mouse monoclonal DYKDDDDK Tag (9A3, Cell Signaling) antibody (named anti-FLAG in the text) was used at a 1:2000 dilution. The rabbit monoclonal anti-NAP1 C-terminal (EPR14698, Abcam) antibody was used at a 1:100 dilution for IF staining and 1:1000 for WB analysis. The rabbit polyclonal anti-SINTBAD (#ab106394, Abcam) was used at a 1:50 dilution. The rabbit polyclonal anti-TANK (#ab47632, Abcam) antibody was used at a 1:50 dilution for IF staining without success. The rabbit polyclonal anti-OPTN (#PA5-51882, Thermo Fisher Scientific) antibody was used at a 1:100 dilution. The rabbit polyclonal anti-TRIF (#PA5-88150, Thermo Fisher Scientific) antibody was used at a 1:500 dilution. The rabbit monoclonal anti-LC8 (EPI660Y, Abcam) antibody was used in WB at a 1:1000 dilution. The rabbit polyclonal anti-STAT1 (E−23, Santa Cruz) antibody was used in WB at a 1:1000 dilution. The rabbit polyclonal anti-MAVS (#A300-782A, Bethyl laboratories) antibody was used at a 1:2000 dilution.

Secondary fluorescent antibodies for IF staining were purchased from Molecular Probes (Alexa fluor 488-, 568-, or 647- conjugated). Secondary fluorescent antibodies for WB analysis were purchased from Cell Signaling (Fluor 800-conjugated IgG or Fluor 680-conjugated IgG). Secondary antibodies coupled to horseradish peroxidase (HRP) for WB analysis after co-IP were purchased from Invitrogen (Anti-Rabbit IgG secondary antibody, HRP) and from Sigma (Anti-Mouse IgG secondary antibody, HRP).

The MitoTracker Red CMXRos (Cell Signaling) was used at 50 nM final concentration. The FM4-64FX lipophilic styryl dye (Molecular Probes) was used at a final concentration of 5 μg/mL. 5′ppp-dsRNA was provided by InvivoGen and used at 4 μg/mL final concentration.

Viral infection

Monolayers of cells (from 60 to 80% confluence) were infected at indicated MOI of RABV diluted in TN buffer (137 mM NaCl, 5 mM KCl, 1.8 mM Na_2HPO_4, 25 mM Tris HCl pH 7.5 supplemented with 5% tryptose). After 1h of incubation at room temperature, the inoculum was removed and the cells were maintained in DMEM (or DMEM Fluorobrite, or IMDM) supplemented with 2.5% FCS and incubated at 37°C and 5% CO_2. For "mock" conditions, cells were incubated for 1 h at RT only with TN buffer. In all imaging experiments, the multiplicity of infection (MOI) was 3.

Construction and recovery of recombinant SAD virus expressing mutated phosphoprotein P

The original full-length genomic plasmid SAD L16-B19 was digested with NcoI and SnaBI restriction enzymes (New England Biolabs). Two overlapping fragments were amplified by PCR: the first fragment was going from NcoI site to position 672 in the P coding sequence carrying the S179P mutation and the second fragment was going from position 643 in the *P* gene to the SnaBI site in the *M* gene. The PCR products and the digested genomic plasmid were assembled using Gibson Assembly kit (New England Biolabs) to obtain the resulting plasmid, pSAD-S179P. Recombinant virus was recovered as described previously.[87] Briefly, BSR cells (7×10^5 cells) were transfected using Lipofectamine 2000 (Invitrogen) with 10 μg of genomic plasmid pSAD-S179P, in addition to 5 μg pTit-N, 2.5 μg pTit-P, 2.5 μg pTit-L, and 1.25 μg pTit-G, which encode the N, P, L, and G proteins of rabies virus strain SAD L16-B19. These plasmids were co-transfected with 1.5 μg of a plasmid expressing the T7 RNA polymerase. Eight days post-transfection, the

supernatant was passaged on fresh BSR cells, and the recombinant viruses were amplified for four days to constitute a pre-stock which was titrated by IF staining with anti-P or anti-N antibodies. This pre-stock was used to infect BSR cells (MOI = 0.1). The supernatant was collected after 4 days, aliquoted and stored at −80°C for further experiments. The P gene was also sequenced, which did not reveal any mutation other than S179P.

Titration of SAD and SAD-S179P viruses

BSR, N2A and U-373MG cells were infected at MOI 0.05 or 3 by SAD or SAD-S179P for 12 h, 16 h, 24 h, 48 h or 72 h. Viral supernatants (1mL of final volume) were clarified at 5,000g for 10 min and stored at −80°C prior titrations. For titrations, BSR cells were infected with 100 μL of the viral supernatants at different dilutions for 16 h. Cells were then fixed with 4% PFA and stained with the anti-P antibody and DAPI. The percentage of infected cells was determined using fluorescence microscopy and the ImageJ software[84] to calculate titers of each viral stock.

Luciferase assay

HEK293T cells were seeded in 24-well plates at a cell density of 1.5×10^5 per well and transfected the next day using lipofectamine 2000 (Invitrogen). In all experiments, cells were co-transfected with 20 ng of pRL-TK plasmid coding the Renilla luciferase as internal control. For reporter gene assay in *P* gene transfected cells, cells were co-transfected with 60 ng of empty plasmid or P plasmids (either pP_{SAD}, pP_{CVS}, pP_{CSV}-P179S, or pP_{SAD}-S179P), 120 ng pIFN-β-Luc containing firefly luciferase under the control of full-length IFN-β promoter and 120ng of pEF6FLAGΔRIG-I,[33] or pIRF3-5D,[35] or pGFP-hTBK1, or phTBK1. For reporter gene assays in virus-infected cells, HEK293T were infected (MOI = 2) at 6 h post-transfection with pIFN-β-Luc. Twenty-four hours post-transfection cell lysates were prepared and subjected to reporter gene assays and WB analysis. The lysates were analyzed using the dual-luciferase reporter assay (Promega). Each experiment was performed in triplicate. For each sample, the firefly luciferase fluorescence units were normalized to Renilla luciferase fluorescence units and the mean fold induction of firefly luciferase was compared to that in non-stimulated cells (not transfected with pEF6FLAGΔRIG-I).

Quantification of the expression of endogenous *IFN-β* gene

Human U-373MG and murine N2A cells were infected at MOI 3 by SAD or SAD-S179P viruses for 8 h, 12 h or 16 h. Cells were lysed and total RNAs from non-infected and infected cells were isolated and purified with the NucleoSpin RNA kit (Macherey-Nagel) following manufacturer's instructions. Amount and purity of extracted RNAs were assessed spectroscopically and 500 ng of total RNAs were used to synthesize complementary DNAs (cDNAs) using the High Capacity cDNA Reverse Transcription Kit (Thermo Fischer Scientific). Human *IFN-β* and *GAPDH* cDNAs were quantified by qPCR using the Power SYBR Green Master Mix (Thermo Fischer Scientific) and specific primers. The $2^{-\Delta Ct}$ method was used to quantify the relative quantity of IFN-β mRNA to GAPDH mRNA.

Western blot analysis

HEK293T cells extracts were prepared using Passive cell Lysis Buffer (Promega) according to the supplier's instructions. For TBK1 detection, N2A cells were directly lysed in Laemmli buffer at 95°C. For HAP1 cells, cells were solubilized in 50 mM Tris-HCl pH7.4, 150 mM NaCl, 1% Triton X-100 and a cocktail of protease inhibitors (#11-836-170-001 Roche Diagnostic) for 30 min on ice before 10 min centrifugation (16,000 g at 4°C). The supernatant was kept for WB analysis.

Proteins were separated by electrophoresis on 10 or 12% SDS-PAGE and transferred onto a nitrocellulose membrane. The membrane was blocked with 5% skimmed milk or 5% BSA in Tris buffer saline (TBS) for 30 min and incubated overnight at 4°C with the corresponding antibodies in TBS supplemented with 0.1% Tween 20 and 1% skimmed milk or 1%BSA. The blots were then washed extensively in TBS - 0.1% Tween 20 and incubated for 1 h with Fluor-conjugated IgG secondary antibodies at room temperature (RT). After washing, the membranes were scanned with the Odyssey infrared imaging system (LI-COR, Lincoln, NE).

Immunoprecipitation for LC-MS/MS analysis

HEK293T cells (1.4×10^7 cells) were transiently co-transfected with pEF6ΔRIG-I and pcDNA3.1 plasmids encoding flagged version of P protein (either WT or mutant) using Lipofectamine 2000 (11.25 μg DNA of each plasmid). Cells were harvested 24h post-transfection and lysed in buffer containing 50 mM Tris-HCl pH7.4, 150 mM NaCl, 0.5% NP40, 1 mM NaF, 1 mM PMSF and a cocktail of protease inhibitors (#11-836-170-001 Roche Diagnostic). Samples were incubated for 30 min on ice and cleared by centrifugation (16 000g, 10 min, 4°C). Lysates were subjected to immunoprecipitation using anti-FLAG M2 magnetic beads (Sigma Aldrich) previously equilibrated with a buffer containing 50 mM Tris-HCl pH7.4, 150 mM NaCl and 0.05% NP40 for 2h at 4°C on a rotary wheel. Magnetic beads were washed three times with the same buffer. The beads were resuspended in H_2O before mass spectrometry analysis.

LC-MS/MS acquisition

For P_{SAD} (resp. P_{CVS}) samples were digested by trypsin (0.2 μg/μL) in 25 mM NH_4HCO_3 buffer overnight at 37°C. Samples were desalted using ZipTip C18 Pipette Tips (Thermo Fisher Scientific) and analyzed by an Orbitrap Tribrid Fusion (resp. Orbitrap Q-exactive Plus) mass spectrometer in positive mode (Thermo Fisher Scientific) coupled to a Nano-LC Proxeon 1200 (resp. 1000) equipped with an NSI EASY-spray ion source (Thermo Fisher Scientific). Peptides were separated by liquid chromatography with the following

parameters: Acclaim PepMap100 C18 pre-column reversed phase (2 cm, 3 μm, 100 Å), EASY-spray C18 column reversed phase (P/N ES805A, 75 cm, 75 μm i.d., 2 μm, 100 Å), 300 nL/min flow rate, gradient from 95% solvent A (water, 0.1% formic acid) to 40% (resp. 35%) solvent B (80% - resp. 99.9% - acetonitrile, 0.1% formic acid) over a period of 120 min (resp. 98 min), followed by a column regeneration of 20 min, giving a total run time of 140 min (resp. 118 min). Peptides were analyzed in the Orbitrap cell, in full ion scan mode, at a resolution of 120,000 (resp. 70,000) with a mass range of m/z 350-1550 (resp. 375-1500) and an AGC target of 4.10^5 (Resp. 3.10^6). For $P_{SAD,}$ fragments were obtained by Higher-energy C-trap Dissociation (HCD) activation with a collisional energy of 27%, and a quadrupole isolation window of 1.6 Da. MS/MS data were acquired in the Ion trap in a Top-Speed mode with 3 s cycles, with an AGC target of 1.10^4 and with a dynamic exclusion of 60 s. The maximum ion accumulation times were set to 100 ms for MS acquisition and 35 ms for MS/MS acquisition.

For P_{CVS}, fragments were obtained by HCD activation with a collisional energy of 27%, and a quadrupole isolation window of 1.4 m/z. MS/MS data were acquired in the Orbitrap with a resolution of 17,500, a TopN of 20, with an AGC target of 2 × 105 and with a dynamic exclusion of 30 s. The maximum ion accumulation times were set to 50 ms for MS acquisition and 45 ms for MS/MS acquisition.

LC-MS/MS data processing

Data were processed with the PEAKS Online Xpro software (Bioinformatics Solutions Inc., Waterloo, ON, Canada). Raw MS data were searched against the Homo Sapiens UniProtKB 2021_03 protein database (reviewed, 20,371 entries) with addition of P_{SAD} and P_{CVS} bait sequences. The precursor and product ion tolerances of peptides were set at 20 ppm and 0.05 (for P_{CVS}) or 0.5 Da (for P_{SAD}) respectively. The digest mode of trypsin was set as specific with 2 missed cleavages and the max variable PTM per peptide was set at 3. Oxidation (+15.99), deamidation (+0.98) and phosphorylation (+79.97) were specified as variable modifications and half of a disulfide bridge (−1.01) as a fixed modification. Protein/peptide quality identification was ensured using built-in filters, especially a false-discovery rate (FDR) of 1% was applied at both peptide and protein levels. In addition, the PEAKS Q module was used for label-free quantification (LFQ) of the digested peptides generated under various experimental conditions. Qlucore Omics Explorer software version 3.7 (Qlucore AB, Lund, Sweden) was used for statistical analysis and processing of LFQ data.

The mass spectrometry proteomics data have been deposited to the ProteomeXchange Consortium via the PRIDE partner repository[82] with the dataset identifier PXD028740.

Co-immunoprecipitation of TBK1 with P protein

N2A cells (6.5×10^5 cells) were infected with either SAD or SAD-S179P. 16 h post-infection, cells were incubated with 300 μM DSP (Thermo Fisher Scientific) in phosphate buffer saline (PBS) for 30 min at room temperature. The reaction was then stopped with 20 mM glycine pH 7.4 in PBS for 15 min at room temperature. Cells were then lysed in 250 μL buffer containing 50 mM Tris-HCl pH7.4, 150 mM NaCl, 0.5% NP40, 1 mM NaF, 1 mM PMSF and a cocktail of protease inhibitors (Roche Diagnostic). Samples were incubated for 30 min on ice and cleared by centrifugation (16,000g, 10 min at 4°C). 10 μL were set aside for direct loading and WB analysis. Lysates were incubated with mouse monoclonal anti P antibody 31G10 at 4°C for 1.5 h on a rotary wheel before incubation with magnetic protein A beads (Pierce) for 1.5 h at 4°C on a rotary wheel. Magnetic beads were washed three times with the lysis buffer before resuspension in Laemmli buffer (containing 5% β-mercaptoethanol) prior to WB analysis.

Yeast two-hybrid (Y2H) system

The proteins N, hTBK1 as well as phosphorylation mutants hTBK1-S172A and hTBK1-Y179A (preys) were fused to the sequence encoding the GAL4 activation domain (GAL4-AD) and were used to test the interaction with the different P (baits), inhibitory and non-inhibitory, which were fused to the DNA-binding domain of LexA (LexA-BD). The yeast L40 strain containing the reporter gene *lacZ* was transformed with the prey plasmids pGAD-N, pGAD-hTBK1, pGAD-hTBK1-S172A, pGAD-hTBK1-Y179A and the different bait plasmids pLex-P by using a lithium acetate protocol. Double transformants were grown on plates containing medium lacking Trp and Leu (Trp2 Leu2) to select for the presence of both the bait and the prey. Positive clones were then assayed for β-galactosidase activity. Interaction between baits and preys conferred the ability to grow on L40 in the absence of histidine (through induction of the HIS3 gene) and to express β-galactosidase, by reconstitution of transcription factor for *lacZ* gene.

Yeast protein extraction

From a one-day liquid culture, L40-transformed yeasts were pelleted (3 min at 1900g) and washed twice in cold water. Then, one volume (equal of the pellet volume) of glass beads was added in addition to a lysis buffer (50 mM Tris-HCl pH8, 300 mM NaCl, 0.5% SDS, 12 mM EDTA pH8, 10 mM DTT, 1 mM NaF, 1 mM PMSF, 0.5 mM Na3VO4 and a cocktail of protease inhibitors). The yeast wall rupture was mechanically achieved by 4 cycles of vortexing of 30 s with 30 s in ice between each. After a centrifugation of 10 min at 10 000 g at 4°C, protein concentration in the supernatant was measured by Bradford assay (Bio-Rad) before WB analysis.

Immunofluorescence staining and confocal microscopy

Cells were fixed either for 10 min at −20°C with 37.5% methanol and 50% acetone before rehydratation for 3 min in PBS or, when indicated, for 15 min at RT with 4% paraformaldehyde (PFA) and further permeabilized for 5 min with 0.1% Triton X-100 in PBS. After saturation with 1% BSA in PBS, cells were incubated with the indicated primary antibodies for 1h at RT, washed and incubated for

45 min with Alexa fluor conjugated secondary antibodies. Cells were then incubated for 5 min with 0.1 μg/mL DAPI in PBS (to stain the nuclei) before washing and mounting with Immu-mount (Thermo Fisher Scientific). Images were sequentially acquired using a laser scanning SP8 confocal microscope (Leica) with a 63x oil immersion objective (HC Plan Apo, NA: 1.4, Leica). We used 405, 488 and 561 nm wavelengths to excite DAPI, GFP and mCherry respectively and their fluorescence was collected through the following bandpass 415-455, 500-540 and 575-625 nm.

Quantification of TBK1 condensates

The number of TBK1 (or GFP-mTBK1) condensates was determined using ImageJ software. Analyzed micrographs corresponded to median sections of infected cells. First of all, cells outlines were drawn and nuclei cropped to conserve only the cytoplasm. Then, images were converted into 8-bit before applying a threshold allowing the isolation of each TBK1 condensate. A similar threshold was used for the isolation of NBs. The value of thresholds was the same between all images to allow comparisons. Finally, the « analyze particles » plug-in was used to count the total number of TBK1 condensates (and NBs) per infected cell. We correlated these results to determine the proportion of TBK1 condensates that colocalized with NBs. We also determined the proportion of TBK1 condensates harboring a ring-like structure. For each condition, at least 50 random infected cells were analyzed per independent experiment (at least 3 independent experiments)

Live cell microscopy

For live cell imaging, N2A cells were seeded on 35 mm Glass Bottom μ-Dish (Ibidi). After 24h of growth, cells were infected, or mock-infected, with SAD or SAD-S179P recombinant virus in DMEM FluoroBrite medium (Gibco-Life Technologies) supplemented with 2.5% FCS and antibiotics. When indicated, after 1 h of adsorption at RT, cells were transfected using Lipofectamine 2000 with plasmids encoding the proteins of interest fused to either GFP or mCherry. When cells were only transfected (i.e. non-infected), the medium was supplemented with 10% FCS and antibiotics. Cells were then incubated at 37°C and 5% CO_2 and maintained in these conditions during imaging.

For mitochondria labeling, N2A cells were infected with RABV SAD (MOI = 3) and transfected with pGFP-mTBK1 after virus adsorption. after 15 h of infection, cells were incubated with 50 nM MitoTracker Red CMXRos for 30 min at 37°C in presence of 5% CO_2, and then the medium was changed. One hour after addition the dye, live cells were analyzed by epifluorescence microscopy.

The lipophilic probe FM4-64FX was used to label the cellular membranes. N2A cells were infected with RABV SAD (MOI = 3) and transfected with pGFP-mTBK1 immediately after virus adsorption. After 12 h of infection, cells were incubated with 5 μg/mL of FM4-64FX for 4 h at 37°C in presence of 5% CO2. Live cells were then analyzed by epifluorescence microscopy.For live cell imaging, HAP1 cells were seeded on 35 mm Glass Bottom μ-Dish (Ibidi). After 24 h of growth, the culture medium was replaced by DMEM Fluorobrite medium supplemented with 2.5% FCS (without antibiotics) and cells were transfected using Lipofectamine 3000 (Invitrogen) with plasmids encoding the proteins of interest fused to either GFP or mCherry. Cells were then incubated at 37°C and 5% CO_2 and maintained in these conditions during imaging.

Data acquisition was performed either on an AxioObserver epifluorescence microscope (Zeiss), or a spinning disk microscope (Gataca systems). Widefield observations were performed with a 63x oil immersion objective (Plan. Apochromat, NA: 1.4, Zeiss) and dedicated filter cubes for GFP (ex: 475/40, em: 530/50) and mCherry (ex: 545/25, em: 605/70). Images obtained with the epifluorescence microscope that are shown in the figure have been deconvolved using the Huygens Imaging software (Scientific Volume Imaging).

The spinning disk microscope was composed of a CSU-X1 confocal scanner unit (Yokogawa), an Eclipse Ti E inverted microscope body (Nikon), and a 100x objective (Apochromat TIRF oil-immersion, NA: 1.49). Blue (488 nm,Vortran, 150 mW) and Yellow (561 nm,Coherent, 100 mW) lasers were used for excitation of GFP and mCherry, respectively. A quad-band dichroic mirror (405/491/561/641 nm, Chroma) was used and bandpass filters of 525/45 nm and 607/36nm (Semrock) allowed the sequential detection of GFP and mCherry, respectively. Images were recorded with a Prime 95B sCMOS camera (Photometrics). The whole system was driven by MetaMorph software version 7.7 (Molecular Devices).

Image processing and analysis

Before quantification, images were deconvolved using Huygens software (Scientific Volume Imaging). We used Imaris v9.3 (Bitplane) to generate 3D rendering of TBK1 and NAP1 condensates and to quantify their volume and sphericity. The impact of the spherical aberration artifacts is limited by applying on the data a correction factor of 0.85 along the z axis (according to the focal shift correction factor obtained[89]). For tracking experiments, maximal intensity projections of 3μm z-stacks were analyzed with FIJI[85] using the TrackMate plugin[90] with the following parameters (Detector: Laplacian of Gaussian; Tracker: Linear Assignment Problem). Particle speed is directly extracted from TrackMate measurements, while trajectory straightness is calculated by dividing the particle displacement by the trajectory length.

FRAP experiments

FRAP experiments were performed on N2A cells transfected either with pGFP-mTBK1 and pmCherry-mNAP1, or infected with RABV SAD (MOI = 3) and, immediately after virus adsorption, transfected with pGFP-mTBK1 and pP-mCherry. Data acquisition was performed on an inverted Nikon Ti Eclipse E microscope coupled with a Spinning Disk (Yokogawa CSU-X1) and a 100x objective

(Apochromat TIRF oil-immersion, NA: 1.49). Blue (488 nm, Vortran, 150 mW) and Yellow (561 nm, Coherent, 100 mW) lasers were used for excitation of GFP and mCherry, respectively. A quad-band dichroic mirror (405/491/561/641 nm, Chroma) and band-pass filters of 525/45 nm and 607/36 nm (Semrock) were used to ensure spectral separation. Images were recorded with a Prime 95B sCMOS camera (Photometrics). FRAP experiments were performed using iLas 2 module (GATACA Systems) and the whole system was driven by MetaMorph software version 7.7 (Molecular Devices). FRAP experiments on ring-like structures were performed at the frame rate of 1 image every second using the following sequence: 3 s of pre-bleach, 10-15 ms or 40-60 ms to bleach GFP-mTBK1 or mCherry-NAP1 respectively, 90 s post-bleach. Bleaching was performed in a circular region of 1.4 μm diameter. FRAP experiments for NBs were performed with the following sequence: 6 s pre-bleach, 40 ms to bleach GFP-mTBK1, 120 s post-bleach at a frame rate of 1 image every 500 ms for the first 10 s then every 2 s for 110 s. Bleaching was performed in a circular region (diameters of 2.8 and 1.4 μm for whole NB or subvolumes, respectively).

For the FRAP data analysis we used a home-made macro on FIJI[85] performing the following steps. On every slide, the background was estimated and removed by measuring a region outside the cells. To correct acquisition bleaching, the mean fluorescence measured in the bleached region was normalized by the mean value of a region in a neighboring cell. Then a second normalization was applied by dividing the results by the mean value of the pre-bleach sequence to allow the comparison of the recovery curves.

QUANTIFICATION AND STATISTICAL ANALYSIS

Statistical analysis were performed using Prism (GraphPad software). Data comparison was performed using Student t-test or Kolmogorov-Smirnov test. Statistical details of experiments are indicated in the figure legends. Results are indicated as mean ± SD. For small numbers of independent experiments, all data points were presented.

Cell Reports, Volume *42*

Supplemental information

Rabies virus P protein binds to TBK1 and interferes with the formation of innate immunity-related liquid condensates

Nathalie Scrima, Romain Le Bars, Quentin Nevers, Damien Glon, Guillaume Chevreux, Ahmet Civas, Danielle Blondel, Cécile Lagaudrière-Gesbert, and Yves Gaudin

Supplemental information

Rabies virus P protein binds to TBK1 and interferes with the formation of innate immunity-related liquid condensates

Nathalie Scrima, Romain Le Bars, Quentin Nevers, Damien Glon, Guillaume Chevreux, Ahmet Civas, Danielle Blondel, Cécile Lagaudrière-Gesbert, Yves Gaudin

Figure S1

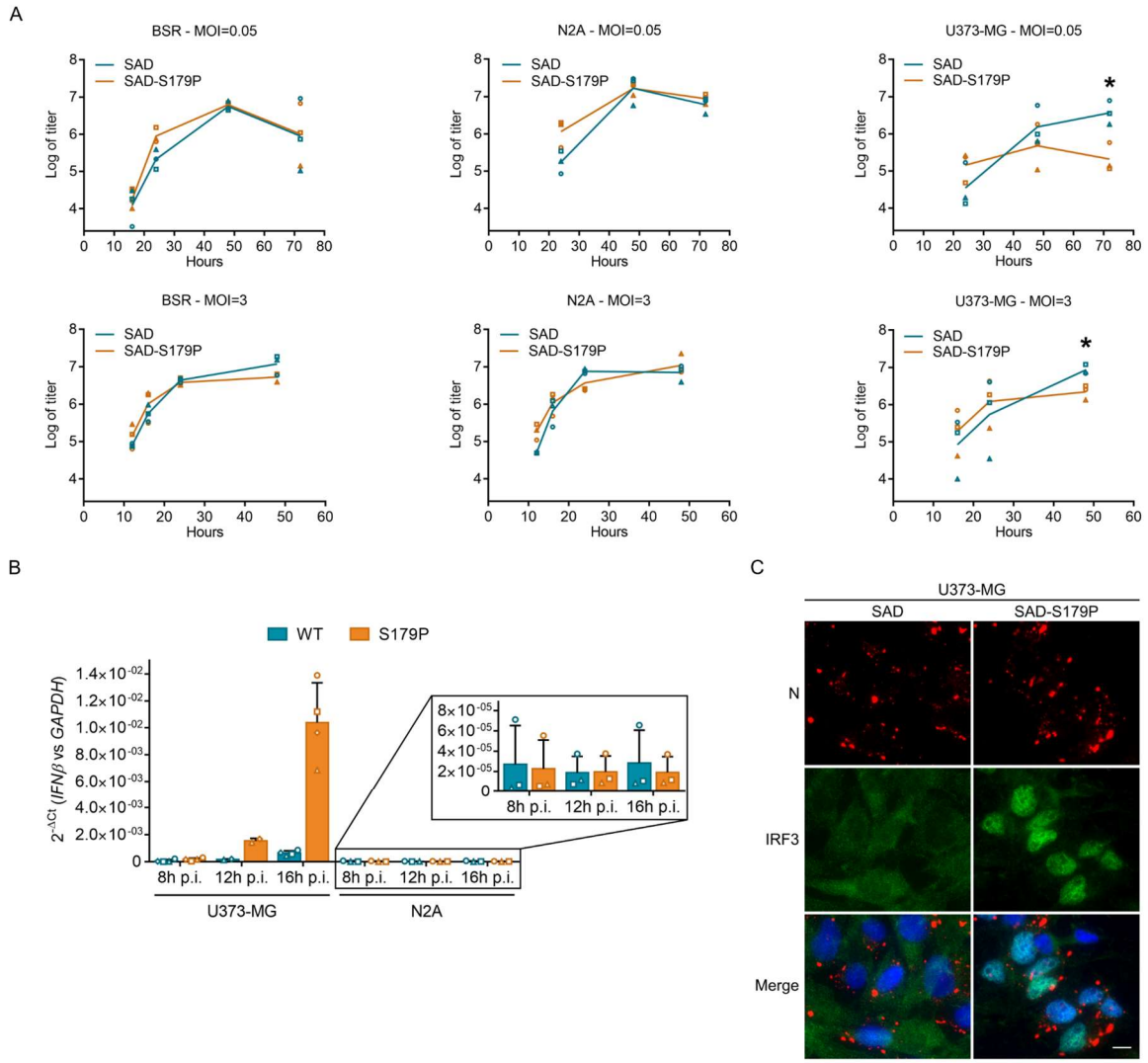

Figure S1. Characterization of RABV SAD and SAD-S179P, Related to Figure 1

(A) Growth curves of SAD and SAD-S179P in BSR, N2A and U-373MG cells at MOI 0.05 and 3. Viral titers were determined in BSR cells. The means of the log10 of the viral titer are indicated as well as the data points corresponding to replicates of 3 independent experiments. Significant differences are indicated (* $P < 0.05$) after application of a Student t-test.

(B) U-373MG and N2A cells were infected with SAD or SAD-S179P viruses (MOI=3). Relative levels of IFN-β mRNA to GAPDH mRNAs were quantified by RT-qPCR. The bars represent the mean ± standard deviation and data points represent replicates of 3 independent experiments. A magnification of the N2A cells results is shown. Error bars indicate standard deviations.

(C) U-373MG were infected with RABV SAD or RABV SAD-S179P (MOI=3). At 18h p.i, cells were fixed by 4% PFA before analysis by IF after co-staining with the mouse anti-N and rabbit anti-IRF3 antibodies followed by incubation with Alexa-568 goat anti-mouse IgG and

Alexa-488 goat anti-rabbit IgG. DAPI (blue) was used to stain the nuclei (merge). Scale bar: 10 μm.

Figure S2

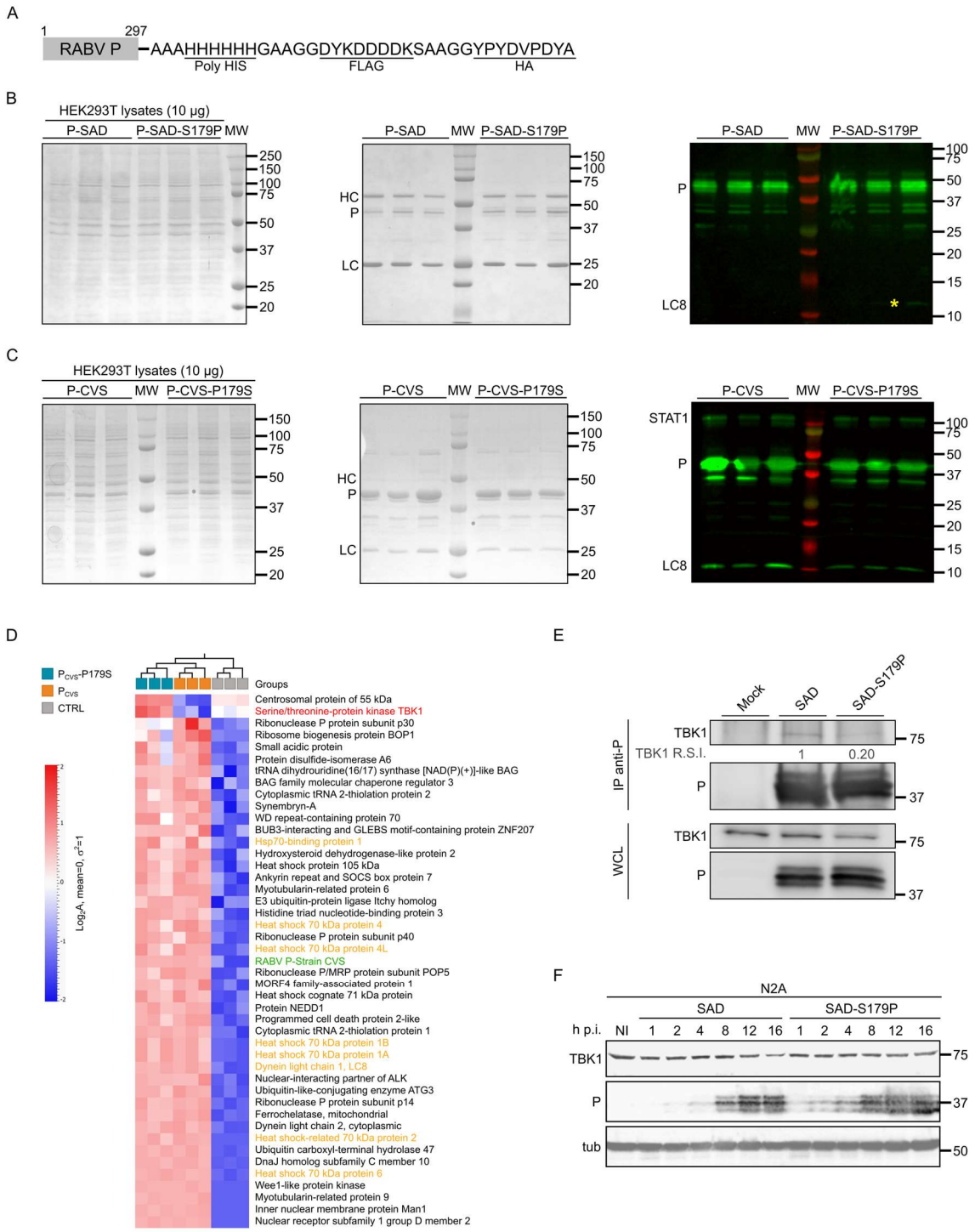

Figure S2. Characterization of RABV P interactome, Related to Figure 2

(A) P constructions used to characterize the interactome of P_{SAD}, P_{CVS}, and their mutants. P constructions have a FLAG tag linked to the C-terminus of P proteins.

(B-C) HEK293T cells were co-transfected for 24 h with plasmids pEF6ΔRIG-I and pP_{SAD}, or pP_{SAD}-S179P **(B)**, or pP_{CVS}, or pP_{CVS}-P179S **(C)**. After cell lysis, 10 µg of total proteins were loaded on gel and stained with Coomassie blue (Left Panels). Cell lysates were incubated with

bead-associated anti-FLAG antibodies before immunoprecipitation. After washing the beads, one tenth of the sample was loaded on a SDS-PAGE and stained with Coomassie blue (Middle panels). Another tenth of the sample was analyzed by WB with anti-P and anti-LC8 antibodies, as well as anti-STAT1 in the case of P_{CVS} (Right panels). In the middle panels, the heavy chain (HC) and light chain (LC) of anti-FLAG antibodies are indicated. The asterisk on the right panel of (**B**) indicates the LC8 protein. The lower molecular weight P bands correspond to isoforms, of which the translation is initiated at AUGs downstream the first AUG by a leaky scanning process[1].

(D) Heatmap comparison of the abundance of proteins associated with P_{CVS} (non-inhibitory form) versus mutant P_{CVS}-P179S (inhibitory form) and control (CTRL), made with Qlucore AB version 3.7. Proteins (>2 unique peptides) were filtered based on a multigroup comparison with p-value<0.005. Abundance data were log2 transformed and standardized with a mean of 0 and variance of 1. A hierarchical clustering was applied on columns and rows were ordered according to PCA component 1 from group comparison. Proteins, of which the name is written in orange, correspond to previously identified P partners. The heatmap is an active plot focused on proteins of higher abundance in P_{SAD} conditions versus the control.

(E) Co-immunoprecipitation of TBK1 with P from infected cells. N2A cells were infected with either RABV SAD virus or RABV SAD-S179P (MOI=3) for 16 h and lysed. Lysates were subjected to immunoprecipitation with the anti-P monoclonal antibody 31G10. Cell lysates (WCL) and immunoprecipitated proteins (IP) were analyzed by WB using monoclonal anti-P and anti-TBK1 antibodies (R.S.I.: relative signal intensity).

(F) N2A cells were either not infected (NI) or infected with RABV SAD or SAD-S179P (MOI=3). At indicated time p.i. cells were lysed and extracts analyzed by WB using anti-TBK1, anti-P, and anti-tubulin antibodies.

Figure S3

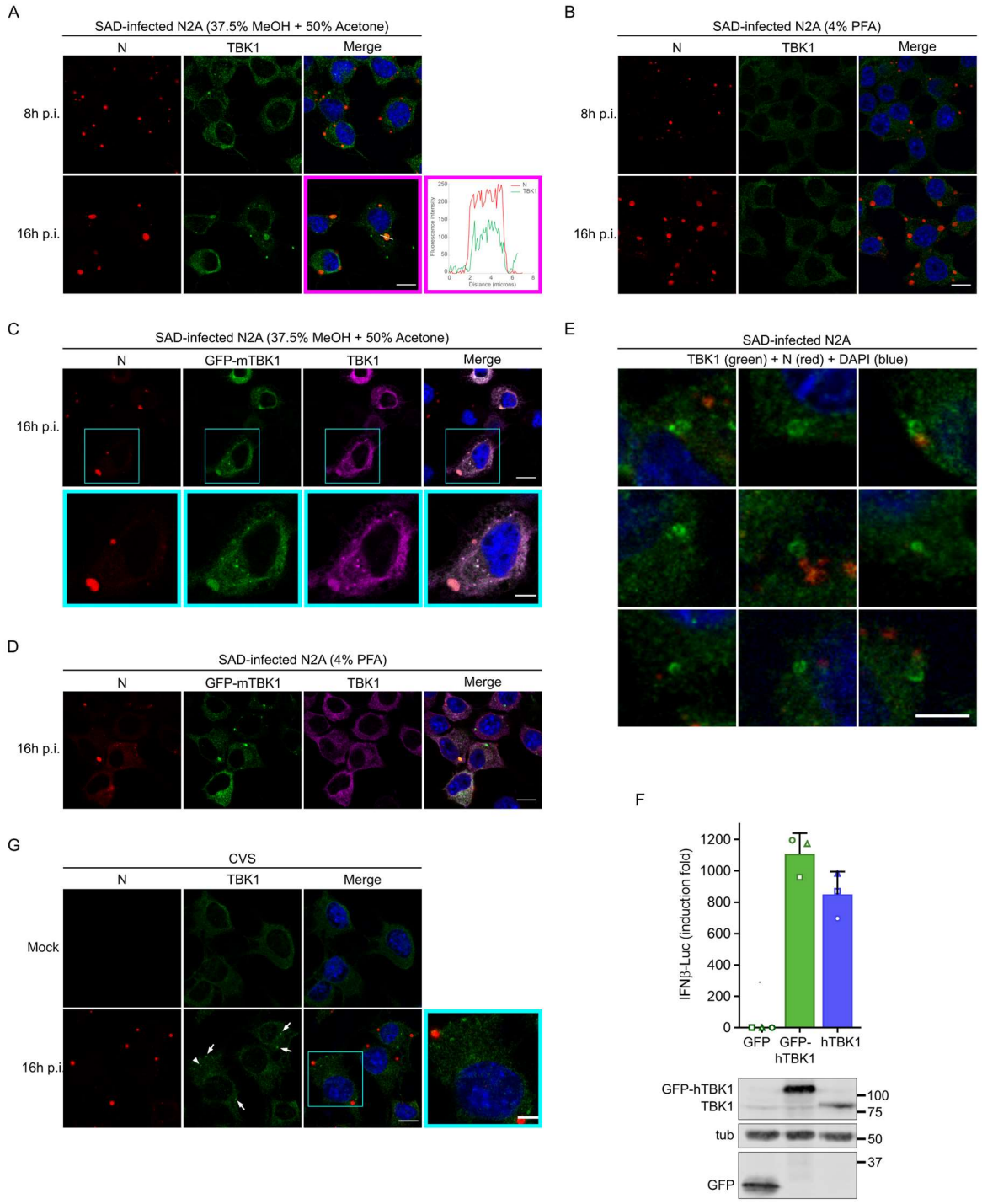

Figure S3. Characterization of the behavior of TBK1 and GFP-TBK1, Related to Figure 2

(A-D) PFA fixation disrupts TBK1 condensates and TBK1 association with NBs

(A-B) N2A cells were infected with RABV SAD (MOI=3). At 8 or 16 h p.i, cells were fixed by methanol/acetone (**A**) or 4% PFA (**B**) before analysis by confocal microscopy after co-staining with the mouse anti-N and rabbit anti-TBK1 antibodies followed by incubation with Alexa-568 goat anti-mouse IgG and Alexa-488 goat anti-rabbit IgG. DAPI (blue) was used to

stain the nuclei (merge). Scale bar: 10 µm. In (A), the fluorescence corresponding to TBK1 (green) and N (red) along the line traced over an NB was quantified by using Image J software and presented on the right of the panel in the magenta box.

(C-D) N2A cells were infected with RABV SAD (MOI=3) and transfected with pGFP-mTBK1 immediately after virus adsorption. At 16 h p.i, cells were fixed by methanol/acetone (**C**) or 4% PFA (**D**) before analysis by confocal microscopy after co-staining with the mouse anti-N and rabbit anti-TBK1 antibodies followed by incubation with Alexa-568 goat anti-mouse IgG and Alexa-647 goat anti-rabbit IgG. DAPI (blue) was used to stain the nuclei (Merge). Scale bar: 10 µm. In (**C**), square boxes are magnified at the bottom of the panel. Scale bar: 5 µm.

(E) Gallery of SAD-induced TBK1 ring-like structures. N2A cells were infected with RABV SAD (MOI=3). At 8 or 16 h p.i, cells were fixed and processed as in (**A**). Images were magnified to show the grainy aspect of the ring-like structures. Scale bar: 5 µm.

(F) HEK293T cells were co-transfected with pIFNβ-luc and plasmids encoding GFP, GFP-hTBK1, or hTBK1. Twenty-four hours after transfection, the cells were lysed. The firefly luciferase activity of each lysate was measured and normalized to the expression of Renilla luciferase. The bars represent the mean fold induction of firefly luciferase compared to non-stimulated cells (transfected with GFP). The lysates were analyzed by WB using anti-GFP, anti-TBK1 and anti-Tubulin antibodies. Data points represent three independent experiments. Error bars indicate standard deviations.

(G) N2A cells were infected with CVS (MOI=3). At 16 h p.i, cells were fixed by methanol/acetone before analysis by confocal microscopy after co-staining with the mouse anti-N and rabbit anti-TBK1 antibodies followed by incubation with Alexa-568 goat anti-mouse IgG and Alexa-488 goat anti-rabbit IgG. DAPI (blue) was used to stain the nuclei (merge). Scale bar: 10 µm.

Figure S4

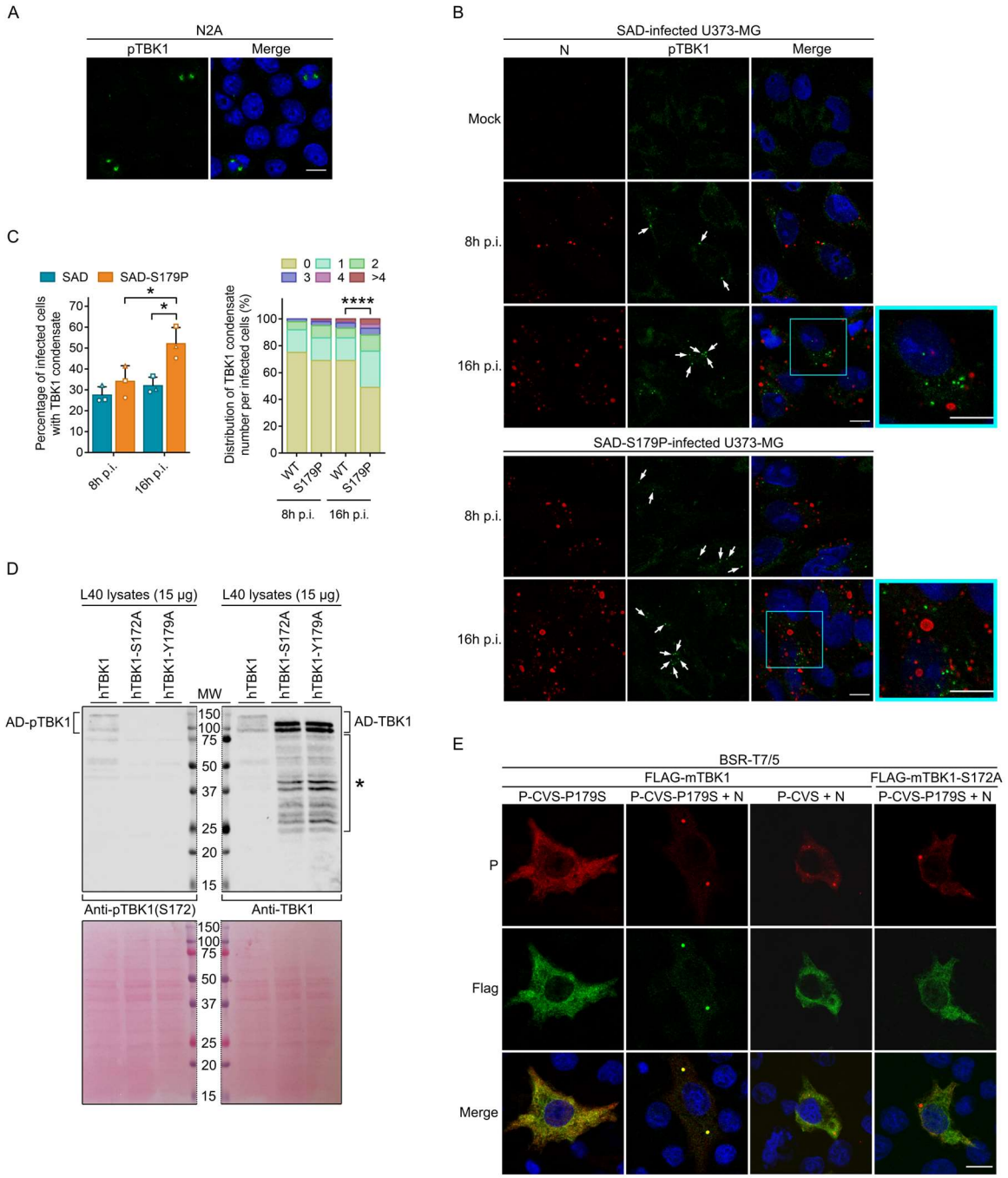

Figure S4. Characterization of TBK1 phosphorylation and its functions, Related to Figure 3

(A) Phosphorylated TBK1 localizes to mitotic spindles. N2A cells were fixed by methanol/acetone before analysis by confocal microscopy after staining with the rabbit anti-pTBK1(S172) antibodies followed by incubation with Alexa-488 goat anti-rabbit IgG. DAPI (blue) was used to stain the nuclei (merge). Scale bar: 10μm.

(B) U-373MG cells were either mock-infected (Mock) or infected with RABV SAD or RABV SAD-S179P (MOI = 3). At 8 or 16 h p.i, cells were fixed by methanol/acetone before analysis by confocal microscopy after co-staining with the mouse anti-N and rabbit anti-pTBK1(S172)

antibodies followed by incubation with Alexa-568 goat anti-mouse IgG and Alexa-488 goat anti-rabbit IgG. DAPI (blue) was used to stain the nuclei (merge). Square box in the merge is magnified on the right of the panel. Arrows indicate TBK1 condensates.

(C) Percentage of infected cells containing TBK1 condensates (left panel) and distribution of the number of condensates per cell (right panel) in cells infected for 8 or 16h by SAD (n=252 and n=370 infected cells respectively from 3 independent experiments) or SAD-S179P (n=259 and n=440 infected cells respectively from 3 independent experiments). p-value were calculated using a Student t-test (for percentage analysis) or a Kolmogorov-Smirnov test (for distribution analysis). All significant differences are indicated. (* $P < 0.05$; **** $P < 0.0001$).

(D) The yeast L40 strain was transformed with either pGAD-hTBK1, pGAD-hTBK1-S172A, or pGAD-hTBK1-Y179A. After lysis, 15 µg of total proteins were loaded on SDS-PAGE for analysis by WB with anti-TBK1 and anti-pTBK1(S172) antibodies (upper panel). The expected molecular weight of hTBK1 (and its mutant forms) fused to AD is 99.3 kDa. The asterisk indicates putative products of degradation. The membrane blot was stained with Ponceau S solution to confirm transfer uniformity (bottom panel).

(E) Association of TBK1 with inclusion bodies formed by co-expression of N_{CVS} and P_{CVS} in the cellular minimal system. BSR-T7/5 cells were co-transfected for 24 h with plasmids pTit-P_{CVS} or pTit-P_{CVS}-P179S, pTit-N_{CVS}, and pTit-FLAG-TBK1-WT or pTit-FLAG-TBK1-S172A. Cells were fixed and analyzed by confocal microscopy after co-staining with the rabbit anti-P and mouse anti-FLAG antibodies followed by incubation with Alexa-568 goat anti-rabbit IgG and Alexa-488 goat anti-mouse IgG. DAPI (blue) was used to stain the nuclei (merge). Scale bar: 10 µm.

Figure S5

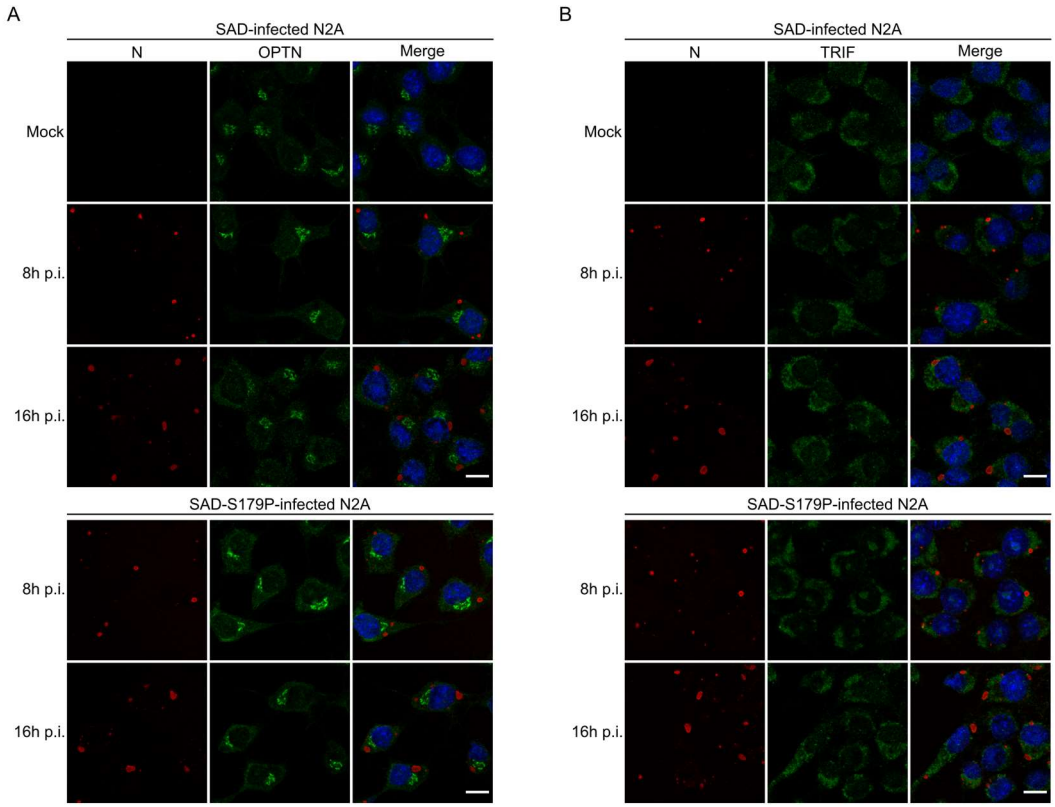

Figure S5. RABV infection does not affect OPTN and TRIF localization, Related to Figure 5 (A-B) N2A cells were either mock-infected (Mock), or infected with RABV SAD (MOI=3), or infected with RABV SAD-S179P (MOI=3). At 8 or 16 h p.i., cells were fixed by methanol/acetone before analysis by confocal microscopy after co-staining with the mouse anti-N and either rabbit anti-OPTN **(A)** or rabbit anti-TRIF **(B)** antibodies followed by incubation with Alexa-568 goat anti-mouse IgG and Alexa-488 goat anti-rabbit IgG. DAPI (blue) was used to stain the nuclei (Merge). Scale bar: 10μm.

Figure S6

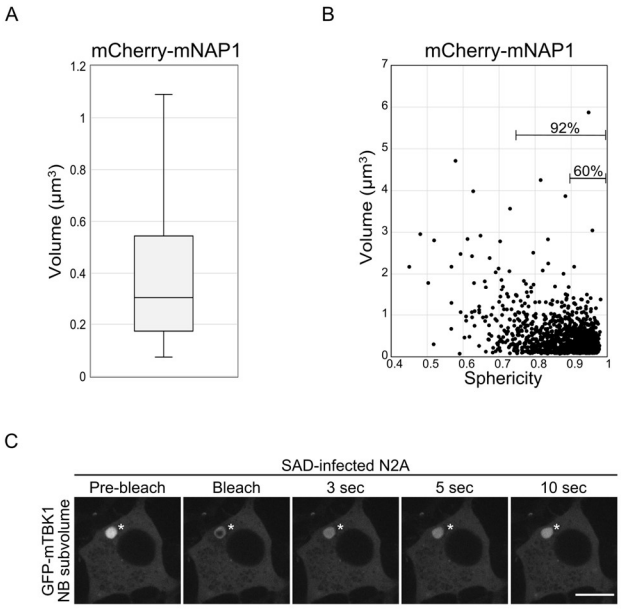

Figure S6. Characterization of mCherry-mNAP1 condensates and of the liquid properties of GFP-mTBK1 in NBs, Related to Figure 7

(A-B) Boxplot representing the volume distribution of the mCherry-NAP1 condensates **(A)** and dot plot representing the relation between the volume and the sphericity of mCherry-NAP1 condensates **(B)** in N2A cells infected with RABV SAD (MOI=3) and co-transfected with pGFP-mTBK1 and pmCherry-mNAP1 (observation 12 h. p.i. ; 55 cells, 1495 particles).

(C) FRAP on GFP-mTBK1 located inside NB. A defined NB subvolume was photobleached. N2A cells were infected with RABV SAD (MOI=3) and, immediately after virus adsorption, transfected with pGFP-mTBK1 and pP-mCherry. FRAP experiment was performed 12h p.i. The diameter of the photobleached region was 1.4 µm. Scale bar: 10 µm.

Figure S7

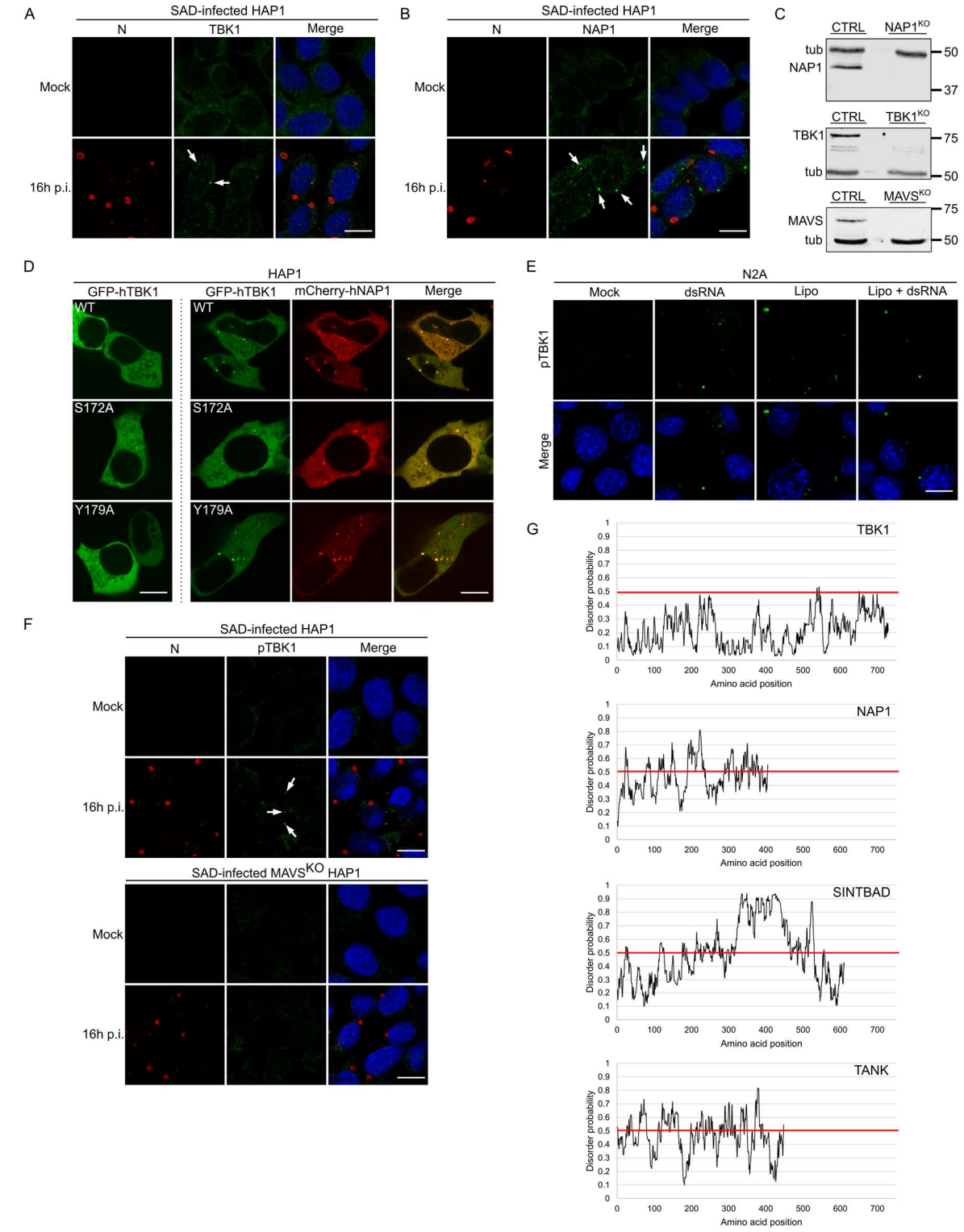

Figure S7. Formation of NAP1 and TBK1 condensates in HAP1 cell line in response to various danger signals, Related to Figure 7 and the Discussion

(A) RABV SAD induces TBK1 condensates formation in HAP1 cells. HAP1 cells were either mock-infected (Mock) or infected with RABV SAD (MOI=3). At 16 h p.i, cells were fixed by methanol/acetone before analysis by confocal microscopy after co-staining with the mouse anti-

N and rabbit anti-TBK1 antibodies followed by incubation with Alexa-568 goat anti-mouse IgG and Alexa-488 goat anti-rabbit IgG. DAPI (blue) was used to stain the nuclei (Merge). Scale bar: 10µm. Arrows indicate TBK1 condensates.

(B) RABV SAD induces NAP1 condensates in HAP1 cells. HAP1 cells were either mock-infected (Mock) or infected with RABV SAD (MOI=3). At 16 h p.i, cells were fixed by methanol/acetone before analysis by confocal microscopy after co-staining with the mouse anti-N and rabbit anti-NAP1 antibodies followed by incubation with Alexa-568 goat anti-mouse IgG and Alexa-488 goat anti-rabbit IgG. DAPI (blue) was used to stain the nuclei (Merge). Scale bar: 10 µm. Arrows indicate NAP1 condensates.

(C) Control of absence of protein expression in HAP1^{KO} cells compared to control parental HAP1 cell line (CTRL). Cells were lysed and extracts analyzed by WB using anti-Tubulin and either anti-NAP1, or anti-TBK1, or anti-MAVS antibodies.

(D) HAP1 cells were co-transfected with either pGFP-hTBK1-WT or pGFP-hTBK1-S172A or pGFP-hTBK1-Y179A, and an empty vector (left panels) or pmCherry-hNAP1 (right panels). At 18 h post-transfection, live cells were analyzed by confocal spinning disk microscopy. Scale bar: 10 µm.

(E) Formation of TBK1 condensates upon N2A cell exposure to danger signal. N2A cells were either mock-treated (Mock), i.e. incubated with the medium without dsRNA or lipofectamine, incubated with the medium containing 4 µg/ml 5'ppp-dsRNA (dsRNA), incubated with the medium containing lipofectamine 2000 alone (Lipo), or transfected with 5'ppp-dsRNA using lipofectamine 2000 diluted in the medium (Lipo + dsRNA). At 6 h post-treatment, cells were fixed by methanol/acetone before analysis by confocal microscopy after staining with the rabbit anti-pTBK1 (S172) antibody followed by incubation with Alexa-488 goat anti-rabbit IgG. DAPI (blue) was used to stain the nuclei (Merge). Scale bar: 10 µm.

(F) MAVS deficiency impedes SAD-induced TBK1 condensate formation. Control parental HAP1 and MAVS^{KO} HAP1 cells were either mock-infected (Mock) or infected with RABV SAD (MOI=3). At 16 h p.i, cells were fixed by methanol/acetone before analysis by confocal microscopy after co-staining with the mouse anti-N and rabbit anti-pTBK1(S172) antibodies followed by incubation with Alexa-568 goat anti-mouse IgG and Alexa-488 goat anti-rabbit IgG. DAPI (blue) was used to stain the nuclei (Merge). Arrows indicate TBK1 condensates. Scale bar: 10 µm.

(G) Identification of putatively intrinsically disordered regions of murine TBK1, NAP1, SINTBAD and TANK using IUPred website (https://iupred2a.elte.hu)[2].

Plasmid name	Gene	N-ter Tag	C-Ter Tag	Mutation	Origin
Cell expression					
pcDNA3.1 hygro(-) backbone					
pP_{SAD}	P (SAD L16 strain)	-	-	-	This paper
pP_{SAD}-S179P	P (SAD L16 strain)	-	-	S179P	This paper
pP_{SAD}-FLAG	P (SAD L16 strain)	-	(His)6, Flag, Tag HA	-	This paper
pP_{SAD}-S179P-FLAG	P (SAD L16 strain)	-	(His)6, Flag, Tag HA	S179P	This paper
pP_{SAD}-mCherry	P (SAD L16 strain)	-	mCherry		This paper
pP_{SAD}-S179P-mCherry	P (SAD L16 strain)	-	mCherry	S179P	This paper
pP_{CVS}	P (CVS N2C strain)	-	-	-	Fouquet et al. (2015)[3]
pP_{CVS}-P179S	P (CVS N2C strain)	-	-	P179S	This paper
pP_{CVS}-FLAG	P (CVS N2C strain)	-	(His)6, Flag, Tag HA	-	This paper
pP_{CVS}-P179S-FLAG	P (CVS N2C strain)	-	(His)6, Flag, Tag HA	P179S	This paper
pGFP-mTBK1	Murine TBK1	GFP	-	-	This paper
pGFP-hTBK1	Human TBK1	GFP	-	-	This paper
pGFP-mTBK1-S172A	Murine TBK1	GFP	-	S172A	This paper
pGFP-hTBK1-S172A	Human TBK1	GFP	-	S172A	This paper
pGFP-mTBK1-Y179A	Murine TBK1	GFP	-	Y179A	This paper
pGFP-hTBK1-Y179A	Murine TBK1	GFP	-	Y179A	This paper
phTBK1	Human TBK1	-	-	-	This paper
pmCherry-mNAP1	Murine NAP1	mCherry	-	-	This paper
pmCherry-hNAP1	Human NAP1	mCherry	-	-	This paper
pGFP-mNAP1	Murine NAP1	GFP	-	-	This paper
pmCherry-mSINTBAD	Murine SINTBAD	mCherry	-	-	This paper
pGFP-mSINTBAD	Murine SINTBAD	GFP	-	-	This paper

pTit backbone					
pTit-P_{SAD}	P (SAD L16 strain)	-	-	-	Finke et al. (1999)[4]
pTit-P_{SAD}-S179P	P (SAD L16 strain)	-	-	S179P	This paper
pTit-P_{CVS}	P (CVS N2C strain)	-	-	-	Nikolic et al. (2017)[5]
pTit-P_{CVS}-P179S	P (CVS N2C strain)	-	-	P179S	This paper
pTit-FLAG-mTBK1	Murine TBK1	Flag	-	-	This paper
FLAG-mTBK1-S172A	Murine TBK1	Flag	-	S172A	This paper
Other backbones					
pEF6-ΔRIG-I	Human Rig-I			Deletion 285-925	This paper
pEF6-FLAGΔRIG-I	Human Rig-I			Deletion 285-925	Yoneyama et al. (2004)[6]
pIRF3-5D	Human IRF3			S396D, S398D, S402D, T404D, S405D	Chang et al. (2006)[7]
pRL-TK	Renilla luciferase				Cat#E2241; Promega
pIFNβ-Luc	Firefly luciferase				Yoneyama et al. (1996)[8]
Two-hybrid system					
pLex-P_{SAD}	P (SAD L16 strain)			-	This paper
pLex-P_{SAD}-S179P	P (SAD L16 strain)			S179P	This paper
pLex-P_{CVS}	P (CVS strain)			-	Raux et al. et al. (2000)[9]
pLex-P_{CVS}-S179P	P (CVS strain)			S179P	This paper
pGAD-N_{CVS}	N (CVS strain)			-	Raux et al. (2000)[9]
pGAD-hTBK1	Human TBK1			-	This paper
pGAD-hTBK1-S172A	Human TBK1			S172A	This paper
pGAD-hTBK1-Y179A	Human TBK1			Y179A	This paper

Table S1. Plasmids used in this study, Related to STAR Methods

References

1. Chenik, M., Chebli, K., andBlondel, D. (1995). Translation initiation at alternate in-frame AUG codons in the rabies virus phosphoprotein mRNA is mediated by a ribosomal leaky scanning mechanism. J Virol *69*, 707-712. 10.1128/JVI.69.2.707-712.1995.

2. Erdős, G., andDosztányi, Z. (2020). Analyzing Protein Disorder with IUPred2A. Curr Protoc Bioinformatics *70*, e99. 10.1002/cpbi.99.

3. Fouquet, B., Nikolic, J., Larrous, F., Bourhy, H., Wirblich, C., Lagaudriere-Gesbert, C., andBlondel, D. (2015). Focal adhesion kinase is involved in rabies virus infection through its interaction with viral phosphoprotein P. J Virol *89*, 1640-1651. 10.1128/JVI.02602-14.

4. Finke, S., andConzelmann, K.K. (1999). Virus promoters determine interference by defective RNAs: selective amplification of mini-RNA vectors and rescue from cDNA by a 3' copy-back ambisense rabies virus. J Virol *73*, 3818-3825. 10.1128/JVI.73.5.3818-3825.1999.

5. Nikolic, J., Le Bars, R., Lama, Z., Scrima, N., Lagaudriere-Gesbert, C., Gaudin, Y., andBlondel, D. (2017). Negri bodies are viral factories with properties of liquid organelles. Nat Commun *8*, 58. 10.1038/s41467-017-00102-9.

6. Yoneyama, M., Kikuchi, M., Natsukawa, T., Shinobu, N., Imaizumi, T., Miyagishi, M., Taira, K., Akira, S., andFujita, T. (2004). The RNA helicase RIG-I has an essential function in double-stranded RNA-induced innate antiviral responses. Nat Immunol *5*, 730-737. 10.1038/ni1087.

7. Chang, T.H., Liao, C.L., andLin, Y.L. (2006). Flavivirus induces interferon-beta gene expression through a pathway involving RIG-I-dependent IRF-3 and PI3K-dependent NF-kappaB activation. Microbes Infect *8*, 157-171. 10.1016/j.micinf.2005.06.014.

8. Yoneyama, M., Suhara, W., Fukuhara, Y., Sato, M., Ozato, K., andFujita, T. (1996). Autocrine amplification of type I interferon gene expression mediated by interferon stimulated gene factor 3 (ISGF3). J Biochem *120*, 160-169. 10.1093/oxfordjournals.jbchem.a021379.

9. Raux, H., Flamand, A., andBlondel, D. (2000). Interaction of the rabies virus P protein with the LC8 dynein light chain. J Virol *74*, 10212-10216. 10.1128/jvi.74.21.10212-10216.2000.